COGNITIVE NEUROSCIENCE

Contextual effects during sensorimotor adaptation are an emergent property of population coding in a cerebellar-inspired model

Tianhe Wang* and Richard B. Ivry

The cerebellum is crucial for sensorimotor adaptation, using error information to keep the sensorimotor system well calibrated. Here, we introduce a population-coding model to explore this process, focusing on how implicit adaptation is modulated by context. The model consists of a two-layered network, designed to capture activity in both the cerebellar cortex and deep cerebellar nuclei. A core feature of the model is that within each layer, the processing units are tuned to both movement direction and the direction of movement error. The model recapitulates a large range of contextual effects such as how prior learning, error uncertainty, or temporal delay affect the rate of adaptation. While these effects have traditionally been taken to indicate a form of meta-learning or context-dependent memory within the adaptation system, the current results show that they can emerge from the population activity of a cerebellar-like hierarchical network that does not represent context.

INTRODUCTION

Humans are incredibly flexible in how we adapt our motor behavior across variable environments. We readily compensate for the added weight of a heavy winter coat when reaching for an object or adjust the force required as we sip on our morning coffee. This form of learning operates implicitly, automatically recalibrating the sensorimotor system without the need for awareness or drawing on cognitive resources (*1*–*3*).

The cerebellum is recognized as playing a key role in this adaptation process (*4*, *5*). Impaired adaptation is one of the hallmarks of cerebellar pathology, observed across a range of tasks from experimentally induced lesions in animal models (*6*–*8*) or neurological disorders in humans (*3*, *9*). Moreover, anatomical and physiological studies have led to computational models in which the cerebellum uses error information to improve subsequent, similar movements (*10*, *11*).

Previous research has suggested that cerebellum-dependent learning is cognitively impenetrable, responding to error in a "rigid" manner even when the correction fails to improve task performance (*1*, *12*–*15*). Moreover, unlike many learning processes, adaptation is not sensitive to the statistical properties of the perturbations (*16*, *17*). However, this view of a rigid, inflexible system has been challenged by recent evidence showing that implicit adaptation is modulated by experience (*18*). For instance, when participants are exposed to a previously experienced perturbation, the rate of relearning is slower than was originally observed (*18*). Not only does this result suggest a degree of flexibility in adaptation but also this context effect is opposite to what is typically observed in studies of relearning: Across a broad range of task domains (e.g., reward-based learning and language acquisition), relearning is typically faster, a phenomenon known as savings (*19*–*21*).

The rigidity and atypical effect of experience point to the need for considering the unique properties of the cerebellum to understand how adaptation is modulated by context and environmental variability. To this end, we develop a computational model of the cerebellum. This model incorporates two core observations from cerebellar physiology. First, studies of oculomotor control have revealed a fundamental tuning property of Purkinje cells (PCs), the primary integrative unit in the cerebellar cortex: These cells are not only tuned to movement direction but also to the direction of error relative to that movement (Fig. 1A) (*22*–*24*). Second, the model includes a two-layered network, with the second layer designed to capture activity in the deep cerebellar nuclei (DCN) (*25*–*28*). We posit that units in the DCN exhibit similar tuning properties as PCs and that units with similar tuning profiles are linked across these two layers (*29*, *30*).

We used the model to generate predictions regarding a range of contextual manipulations and evaluated the predictions with a series of behavioral experiments. Specifically, we systematically examined the effect of past experience, error uncertainty, and variation in temporal dynamics in evaluating our model. Where relevant, we consider several alternative models that have been proposed to elucidate how context and environmental uncertainty modulate sensorimotor learning (*31*–*33*). Our population-coding model provides an excellent fit to the behavioral results even without positing the direct representation of context or latent state variables. Hence, our results present a computational model that illustrates how the hierarchy and dynamics of a cerebellar-like network give rise to a wide range of contextual effects in implicit adaptation.

RESULTS

Cerebellar population-coding model

The basic principles of cerebellar-dependent error-based learning are articulated in the classic Marr-Albus model (*4*, *5*, *34*, *35*). PCs in the cerebellar cortex receive two types of input (Fig. 1A). One source originates in the pontine nuclei. This pathway is hypothesized to provide contextual information, including the target and an efference copy of the motor command. PCs operate as an internal model, using the input to predict the consequences of the motor command (*36*, *37*). The second source originates in the inferior olive (IO) with activation of the climbing fibers, indicating a mismatch between the predicted and expected sensory feedback, a teaching signal that is used to update the internal model.

Department of Psychology and Helen Wills Neuroscience Institute, University of California, Berkeley, Berkeley, CA, USA.
*Corresponding author. Email: tianhewang@berkeley.edu

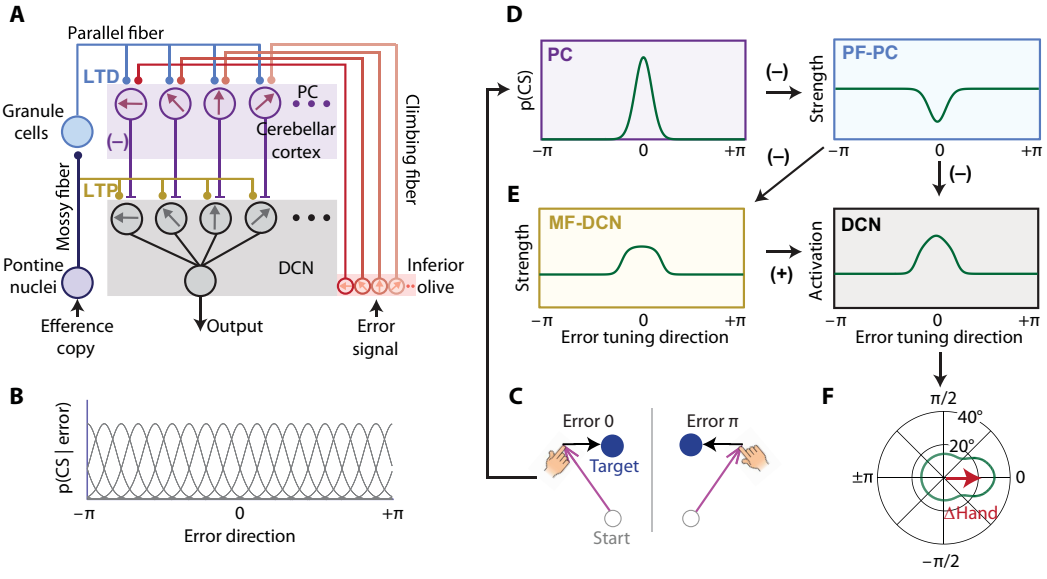

Fig. 1. Illustration of the cerebellar population-coding model. (**A**) Structure of the cerebellar circuit incorporated in the cerebellar population-coding (CPC) model, inspired by Shadmehr (*48*). (**B**) Each Gaussian-shaped curve represents the tuning function of a single PC based on that cell's preferred error direction. For the simulations, we used 1000 units with preferred directions that covered 0-π in a uniform manner. (**C**) Illustration of visual errors, with the direction of the error specified in polar coordinates. (**D** and **E**) Model-generated adaptation in the cerebellar cortex (D) and DCN (E). After experiencing an error in 0 direction, PC with a preferred direction close to 0 will have a high probability of generating a complex spike (CS) [(D); left], which will result in long-term depression (LTD) for active synapses from granule cell inputs to that PC [(D); right]. During the preparation of the next movement, the strength of the input from the parallel fibers (PF) will decrease because of LTD, attenuating the state-space (SS) activity of the PC. We assume that attenuation of the inhibitory PC output to the DCN will facilitate long-term potentiation (LTP) resulting from excitatory mossy fiber (MF) input to the DCN [(E); left]. DCN activation is determined by the excitatory input from the MF and the inhibitory signal from the PC [(E); right]. The frame colors indicate the corresponding pathway in (A). (**F**) DCN population activation plotted in polar coordinates with the resultant vector (purple arrow) showing the change in hand angle. The vector points in the same direction as the error [(C); left] and thus serves to compensate for the error.

Here, we extend the model to provide a general explanation of how learning is modulated by contextual variability. A foundational idea for our model is inspired by a work showing how PCs in the oculomotor cerebellar cortex are simultaneously tuned to both movement direction and the direction of a visual error that arises during that movement (Fig. 1, B and C) (*22*–*24*). Tuning in terms of movement direction is reflected in the simple spike activity of the PCs, and tuning in terms of movement error is reflected in the complex spike (CS) activity of these cells. The latter one induces long-term depression (LTD) of parallel fiber–PC (PF-PC) synapses, reducing the future efficacy of similar input on PC activity (Fig. 1D). Because the two tuning profiles are in opposite directions (*22*, *38*, *39*), error-related activation will result in a change in the output, thus reducing the error.

A second prominent feature of our model is that plasticity occurs within the cerebellar cortex and the DCN (*40*–*43*). Lesion studies of eyeblink conditioning provide one line of evidence indicating that some aspect of consolidated learning is centered in the DCN. Ablation of the cerebellar cortex can completely block de novo cerebellar-dependent learning (*44*). However, once the learned behavior is established, it can persist after lesions to the cerebellar cortex, although the kinematics are disrupted (*45*, *46*). This dissociation can be explained by the dual effect of pontine projections to the cerebellum (*26*, *40*, *47*): a polysynaptic projection through the granule layer to PC and a direct excitatory projection of the mossy fibers (MFs) to the DCN. We assume that PC and DCN neurons are organized such that connections are between units with the same tuning direction (*48*) and that learning in the DCN is gated by learning at the cerebellar cortex (Fig. 1A) (*49*). Specifically, LTD at PF-PC synapses will reduce inhibitory PC input to the DCN, facilitating the emergence of long-term potentiation (LTP) at MF-DCN synapses (Fig. 1E) (*49*, *50*). We note that our assumptions about the locus of LTD and LTP are not critical; one could extend the current model to include LTD and LTP at each layer (see Discussion).

In summary, an error signal will decrease the efficacy of PF input to PCs and increase the efficacy of MF input to the DCN (Fig. 1, D and E). Correspondingly, the net output of the cerebellum will provide a signal of the required change in movement direction to correct for the error (Fig. 1F).

Behavioral task and model parameterization

We first aim to examine the behavior that emerges from the population activity of a network in which the individual units are tuned to both movement direction and the direction of movement error. For the work discussed in this section, a single-layered network with this form of representation is sufficient. In the second half of the Results, we will turn to phenomena that motivate a two-layered network that maps onto the properties of the PCs within the cerebellar cortex and the DCN.

To measure implicit adaptation, we used a variant of a visuomotor rotation task. Participants reached to a visual target, and the feedback, when present, was limited to a cursor. To restrict learning to implicit adaptation, we used task-irrelevant clamped feedback in which the radial position of the cursor was locked to the hand, but the angular position was predetermined for each trial. In most experiments, the cursor was shifted by a constant angle relative to the

target (Fig. 2, A and B) (*1*). Despite being fully informed of the noncontingent nature of the feedback and explicitly instructed to ignore the cursor, the reach angle gradually shifts in the opposite direction of the clamp (*1*, *18*, *51*, *52*). Clamp-induced adaptation has all of the hallmarks of implicit adaptation and, as with other forms of this type of learning, is dependent on the integrity of the cerebellum (*1*, *53*).

To determine the learning and forgetting rates for the units of the cerebellar population-coding (CPC) model, we conducted an initial experiment (Exp 1) in which participants were exposed to 100 trials with clamped feedback (30°), followed by 60 trials without any feedback. We measured the retention rate from the washout block and then fit the learning rate from the training phase. These data were also used to determine the scaling factor, a parameter to transform neural activation into hand angle (Fig. 1F). The CPC model provided an excellent fit of the observed change of hand position (Fig. 2C).

In the following sections, we examine several key predictions derived from the CPC model concerning how the experimental context should modulate implicit adaptation. In Exp 4 (see section "Different retention rates in adaptation"), we distinguish between processing in the cerebellar cortex and DCN. Hence, the full model has a three additional parameters, the learning rate, forgetting rate, and scaling factor for the second layer (with these values estimated from Exp 4; see Materials and Methods). To rigorously test the model, we fixed the values for the six parameters when running simulations to generate predictions for each experiment. Thus, in all of the following simulations, the model predictions are based on parameter values estimated from independent data sets.

Anterograde interference

One basic feature of the CPC model is that, for each unit, learning is fast due to the potent impact of CSs, whereas forgetting in the absence of feedback occurs relatively slowly due to a passive decay process (Fig. 2C). Given the slow rate of forgetting, the population activation will be influenced by the persistent activation of units that were tuned to a recent error. Hence, when the perturbation direction is abruptly reversed, the observed rate of change in performance will be attenuated because of the persistent activation, even if the learning and forgetting rates are invariant in the model (Fig. 2E).

To examine this model prediction, we used a task in which the sign of the clamp was reversed after an initial training block (e.g., 30° followed by −30°; Exp 2; Fig. 2D). Consistent with the model prediction, the results showed that the rate of adaptation was slower in response to the reversed clamp compared to the original clamp (*54*–*58*), a phenomenon known as anterograde interference. Notably, the degree of attenuation closely matched the CPC model's prediction based on the parameter values estimated from Exp 1. These results provide a first example of how a contextual effect can be an emergent result of population coding by the CPC model.

Anterograde interference provides a useful opportunity to compare the CPC model with other computational models that can account for contextual effects in implicit adaptation. The dual state-space (dual SS) model (*21*, *47*) posits that learning involves two processes, one that learns and forgets at a fast rate and a second that learns and forgets at a slow rate (fig. S1A). When the perturbation is reversed, the fast process will quickly respond to the new perturbation and drive adaptation in the opposite direction. However, the slow process will continue to be dominated by its response to the

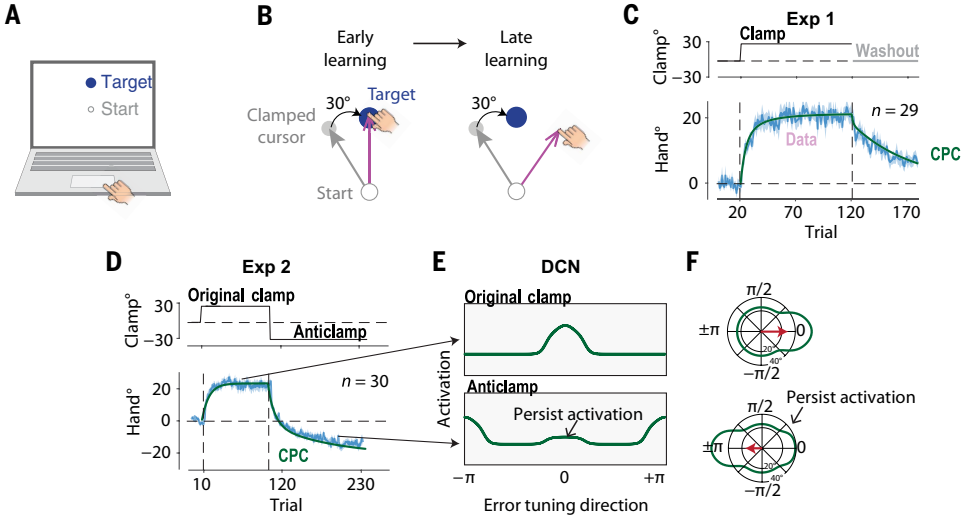

Fig. 2. The CPC model captures learning, forgetting, and anterograde interference during implicit adaptation. (**A**) For online testing, stimuli are presented on the participant's laptop computer, and movements are made on the trackpad. (**B**) For clamped feedback, the angular position of the cursor is rotated by 30° with respect to the target, regardless of the heading direction of the hand. (**C**) Perturbation schedule (top) and results (bottom) for Exp 1. The time course of the mean hand angle is shown in light violet. The CPC model provides a good fit in both the training and no-feedback washout phases. (**D**) To examine anterograde interference, the direction of the clamp was reversed during the training section of Exp 2. The behavioral results show marked anterograde interference. Simulations of the CPC model using the parameters estimated from Exp 1 closely match this result. (**E**) We mark the direction of the 30° clockwise error at 0 in the PC/DCN tuning space and the direction of the opposite (counterclockwise) error as π [also see (F)]. Activation from the original perturbation (top row) persists in the anticlamp training phase (bottom row), indicated by the activation of neurons tuned to 0. This residual memory causes anterograde interference. The shaded area in (C) to (E) indicates standard error. (**F**) The simulation results for the original clamp perturbation (top) and subsequent anticlamp perturbation (bottom) plotted in polar coordinates. The angular axis represents the preferred direction of the units, while the polar axis indicates the strength of their activation. The vector (red arrow) represents the summed activation of all units, which reflects the change in hand angle (Δhand). The length of the vector is shorter in the bottom panel.

original perturbation, thus producing anterograde interference. While the dual SS accounts for anterograde interference by positing multiple processes with different learning rates, the CPC can account for this phenomenon with a single learning and forgetting rate.

Anterograde interference has also been accounted for by models that feature context-dependent learning mechanisms (*32*, *59*, *60*). In these models, a feature or set of features is included to distinguish one context from another, with the degree of interference between contexts being a function of feature similarity. To take a real-world example, the surface of the court is a critical feature for a skilled tennis player, with anterograde interference manifesting when the player finds it challenging to play on a grass surface after having spent a week on clay courts. In the laboratory, context has been manipulated by varying features such as the distribution of target locations, starting position of the movement, type of movement, or form of the perturbation (*59*, *61*, *62*).

This approach is exemplified in the contextual inference (COIN) model (*31*). COIN assumes that the unique features enable the motor system to form separate memories for each context, with the system learning to choose the relevant memory based on the inferred context (fig. S1B). To account for this effect, COIN would first build a memory for the 30° perturbation. With the introduction of the −30° perturbation, the system would create a second, distinct memory. However, there would, at least initially, be some degree of recall of the response to the initial perturbation. Hence, the expressed behavior would be a mixture of memories associated with the initial and second contexts. This would result in a slower rate of learning to compensate for the −30° perturbation compared to the rate of learning observed in response to the original 30° perturbation, one measure of anterograde interference. With the repeated presentation of the −30° perturbation, the system would eventually be biased to consistently infer the new context, allowing learning to reach the same asymptotic level as was observed in response to the 30° perturbation (fig. S1B). In contrast to this inferential process, the CPC model posits that the two perturbations activate different subsets of neurons. Anterograde interference emerges from the pooled activity of the population rather than a competition at recall between distinct memories.

Absence of spontaneous recovery

Having described how different models account for anterograde interference, we next turn to another classic effect that has motivated the COIN and dual SS models, spontaneous recovery. The paradigmatic design to elicit spontaneous recovery is similar to that used to elicit anterograde interference: After initially training participants in response to a perturbation in one direction, the sign of the perturbation is reversed. However, the second perturbation is only present for a limited number of trials, which are required to recalibrate the sensorimotor system such that the reach direction is similar to the baseline (i.e., extinction). Once this state is reached, feedback is removed to examine behavior in the absence of feedback (Fig. 3A) (*21*). Spontaneous recovery refers to the fact that the reaching angle during the no-feedback phase reverts to the direction that had been observed in response to the initial perturbation.

We illustrate how the COIN and dual SS models generate spontaneous recovery in a classic visuomotor task where both implicit and explicit systems can operate (Fig. 3, B and C). By the COIN model, spontaneous recovery occurs in visuomotor rotation tasks because the system recalls, to some extent, the original training context

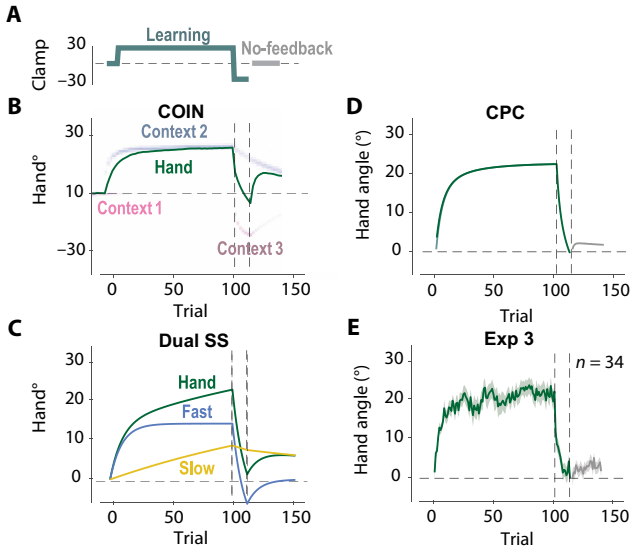

Fig. 3. Implicit adaptation does not exhibit spontaneous recovery. (**A**) A typical training schedule to examine spontaneous recovery: A perturbation in one direction is presented for an extended phase and then reversed for a short phase. The critical test is in the subsequent no-feedback phase. (**B**) COIN simulation in a visuomotor rotation task to illustrate the spontaneous recovery effect: After the reaching angle was being washed out during the reversal perturbation, the movements revert to the direction that in response to the initial perturbation during the no-feedback phase. The light curves showed the state estimation for the baseline context (context 1), original perturbation context (context 2), and the reversal perturbation context (context 3). The shade of color indicates the strength of the context. (**C**) The dual SS model also predicts spontaneous recovery due to the residual state of the slow process. (**D**) The CPC model does not predict spontaneous recovery. It does predict a small rebound at the beginning of the no-feedback phase due to the differential retention rates for the PC and DCN layer, an issue we return to in Exp 5. (**E**) Exp 3 examined the training schedule in (A) but with clamp feedback to isolate implicit adaptation. Empirical results showed no spontaneous recovery in implicit adaptation.

during the no-feedback phase (Fig. 3B). By the dual SS model, spontaneous recovery emerges from the different temporal properties of the two learning mechanisms (Fig. 3C). The state of the fast system will dominate the changes observed after the introduction of the second perturbation, pushing the behavior back toward baseline. However, when the feedback is removed, the state of the slow process is still shifted in the direction induced by the initial perturbation, resulting in spontaneous recovery. In contrast, the CPC model predicts that spontaneous recovery will not occur when learning is restricted to the implicit system because the model does not have a mechanism for context-dependent memory and, in its basic form, has a single parameter for learning rate (Fig. 3D).

To examine whether spontaneous recovery occurs in implicit adaptation, we trained participants in Exp 3 with a 30° clamp in one direction for 100 trials and then presented them with the opposite clamp for 15 trials (Fig. 3A). Pilot testing had shown that a reversal of this duration is sufficient to extinguish the shift in hand angle observed to the initial perturbation. The critical test was the subsequent 30-trial no-feedback block. We failed to observe spontaneous recovery (Fig. 3E and fig. S2B; $t(33) = 1.2$ and $P = 0.23$), a result consistent with the CPC model. These results suggest that spontaneous recovery observed in classic visuomotor rotation tasks (*21*, *31*) may reflect the contribution of explicit processes.

We note that McDougle *et al.* (*63*) used a modified visuomotor task and showed spontaneous recovery during a probe phase designed to isolate implicit learning. However, this phenomenon can be explained by aim-based generalization (*64*) associated with implicit adaptation consistent with the CPC model, rather than the reemergence of a latent state (result S1).

Attenuation in relearning

Savings in relearning is another contextual effect that has been observed in studies of sensorimotor adaptation (*65*, *66*). COIN accounts for savings in the same manner as it accounted for spontaneous recovery (Fig. 4, A and B). The strong memory associated with the initial perturbation will make this a likely candidate for COIN. In a savings design, this inference will accelerate the rate of learning when a previously experienced context is reintroduced.

Savings has also inspired models with meta-learning mechanisms for adaptation (*67*). This idea is central to the Memory of Error (MoE) model (*67*), which posits that the system uses its experience with error to optimize its learning parameters. For example, the learning rate will increase when recently experienced errors are consistent (stable context), whereas the rate will decrease when recently experienced errors are inconsistent. In a savings design, the consistent errors during the original learning increase the learning rate, which results in faster learning when the initial perturbation is reintroduced.

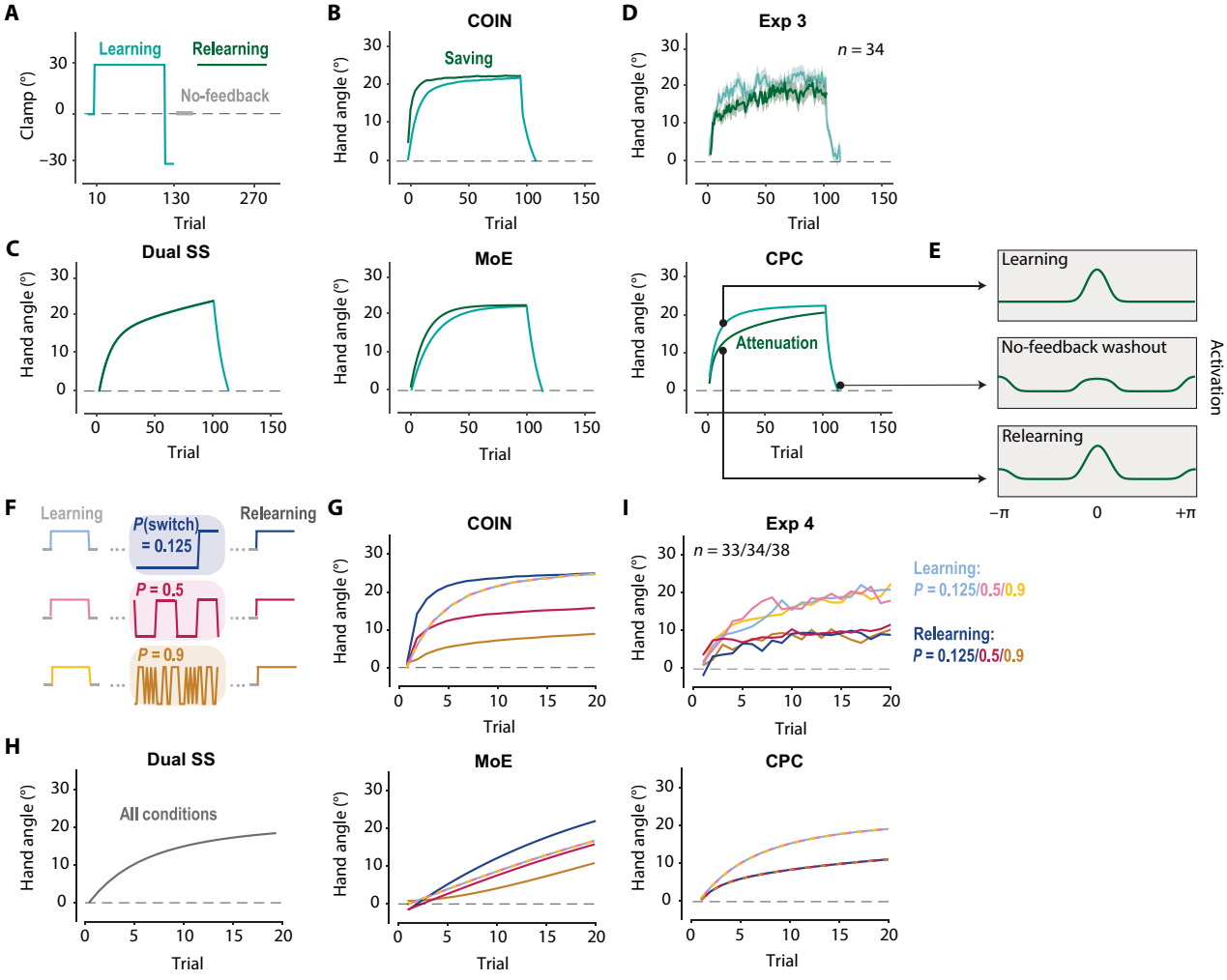

Fig. 4. Context as an emergent property of the CPC model. (**A**) Perturbation schedule in Exp 3 to study relearning. Following the probe of spontaneous recovery (initial learning, reversal, and no-feedback), the original perturbation is reintroduced. (**B**) COIN simulation illustrates a typical savings effect in a visuomotor rotation task. The second learning block (dark) is aligned with the initial learning block (light). (**C**) Simulations of the dual SS, MoE, and CPC models. The dual SS model predicts no savings, the Memory of Error (MoE) model predicts savings, and the CPC model predicts attenuation upon relearning. (**D**) Empirical results show attenuation during relearning, consistent with the CPC model. The shaded area indicates standard error. (**E**) Population activation in the CPC model at three time points (black dots in CPC simulation). While the hand angle is close to zero at the end of the no-feedback washout block, residual activation resulting from the original and reversed clamps is evident in the population, indicated by peaks at 0 and π, respectively (middle). Residual activation from the opposite clamp attenuates relearning (bottom). (**F**) In Exp 4, the learning and relearning phases are separated by a variable phase in which the probability of a perturbation switch is manipulated between participants. (**G**) COIN model simulation shows that the learning rate during relearning would be scaled by the switching rate of the perturbation in a visuomotor rotation task. (**H**) Simulations of the dual SS, MoE, and CPC models. The dual SS model predicts that the learning rate will be identical in learning and relearning regardless of the switching rate. The MoE model predicts that the learning rate in the relearning block will be modulated by the switching rate. The CPC model predicts that, while relearning will be slower than original learning, the learning rate will not be modulated by the switching rate. (**I**) Empirical results are in accord with the CPC model, showing attenuation during relearning that is insensitive to the experienced switching rate.

While savings have been observed in visuomotor rotation tasks, it has been hypothesized that the effect arises solely from the operation of explicit learning processes (e.g., strategy recall) (*18*, *65*). To examine whether implicit learning exhibits savings, we compared two blocks of trials with a 30° clamp in Exp 4, with the second block initiated after a washout period in which the reach angle had returned to the baseline. Savings was assessed by comparing the learning functions in the initial and reexposure phases (Fig. 4A).

To compare the different models, we used this protocol to generate predictions based on simulations of the MoE, dual SS, and CPC models (Fig. 4C). The MoE model produces a savings effect due to an increase in the learning rate when the system recognizes a previously experienced error. The dual SS model predicts that the relearning will be identical to original learning, with no savings or attenuation because the system does not have a memory of the error. In contrast, the CPC model predicts that the rate of relearning will be slower, given that, when the 30° clamp is reintroduced, the state of the population will be altered from the exposure of the system to the opposite error during the washout phase.

We cannot simulate COIN with the error clamp protocol given that the COIN process is based on both the visual feedback and reach angle, and these two sources of information are independent of noncontingent clamped feedback (see Materials and Methods for details). Hence, we replaced the clamped feedback with contingent rotated feedback to simulate COIN. Given this, we include the simulation to visualize how COIN predicts savings with our trial structure in a classic visuomotor rotation task (Fig. 4D).

The behavioral results for Exp 4 are consistent with the predictions of the CPC model, but not the MoE or dual SS models: Adaptation during the reexposure block was slower compared to initial learning (Fig. 4C and fig. S2A; $t(33) = 3.1$ and $P = 0.004$). As suggested by the CPC model, attenuation arises because the state of the population is affected by the feedback experienced during the washout period (Fig. 4E). In the current design, the opposite error used to drive the system back to its baseline state will yield a residual trace at the onset of the reexposure block.

The absence of savings in implicit adaptation is consistent with the claim that savings observed in classic sensorimotor adaptation tasks (*66*, *68*, *69*) may reflect the contribution of explicit processes (*65*). When considered in tandem with the absence of spontaneous recovery, the results suggest that the COIN process central to COIN may be restricted to the operation of explicit processes that contribute to the inference.

Insensitivity to error consistency

The preceding sections highlight two characteristics of implicit adaptation as instantiated in our CPC model. First, classic effects such as spontaneous recovery and savings do not arise from the operation of implicit adaptation. Rather, when the paradigms used to assess these phenomena are modified to isolate implicit adaptation, the observed behavior can emerge from the population activity of units in the CPC model. Second, implicit adaptation is rather rigid, operating in a relatively inflexible manner across contexts. This inflexibility is especially surprising, given that it appears nonoptimal. A priori, one might expect a learning process to be flexible, modifying its parameters in response to the information associated with a given context.

As a further test of this rigidity, we manipulated the consistency of the error in Exp 4 (Fig. 4F). We tested the response to a clamp with a fixed sign (e.g., 30°) before and after a phase in which the sign of the clamp varied across trials. To manipulate consistency, we varied the switching probability in the variable phase, setting it to 12.5, 50, or 90% in a between-subject manipulation. In classic adaptation studies, the response to the error is stronger when the error is more consistent, an effect taken to indicate that the system is sensitive to context. By the COIN model, the system would be less responsive to the error when the context frequently changes (Fig. 4G). However, these contextual effects may only be relevant when considering the contribution of an explicit learning process.

As with savings, we simulated the MoE, dual SS, and CPC models with our experimental trial structure to derive each model's predictions when learning is restricted to implicit adaptation. To this end, we focus on a comparison of the behavior during the first and second fixed perturbation blocks, asking how performance in the latter is affected by the consistency manipulation in the intervening block. MoE predicts that the rate of relearning will inversely scale with switching frequency (Fig. 4H); at low switch rates, the system increases the learning rate and vice versa. The dual SS model predicts that relearning will be identical to that observed during the initial learning phase for all conditions because it has no memory of error. In contrast, the CPC model predicts that the rate of relearning will be lower during the relearning phase compared to original learning, another manifestation of anterograde interference resulting from the opposite errors experienced in the variable-clamp block. This attenuation will be independent of switching frequency. We include COIN to visualize its predictions, but here, we again used a contingent visuomotor rotation on perturbation trials.

The behavioral results were aligned with the predictions of the CPC model. Relearning was markedly slower during the relearning phase compared to original learning (Fig. 4I and fig. S2C; $F(1,101) = 37.7$ and $P < 0.001$). Moreover, the learning rate during the relearning phase was not modulated by the switching rate during the preceding variable phase ($F(2,101) = 0.18$ and $P = 0.84$).

To summarize, Exps 2 to 4 explored a variety of behavioral phenomena observed in studies of sensorimotor adaptation using clamped feedback to restrict learning to implicit adaptation. Consistent with the CPC model, the results indicate that implicit adaptation does not generate classic contextual effects such as spontaneous recovery, savings, and sensitivity to uncertainty. The observed behavior is modulated by recent error history, but these effects can be accounted for by the model's population activity. Hence, the model offers a parsimonious explanation of how perturbation history can influence adaptation without positing context-dependent memory or meta-learning processes (Table 1).

Tuning properties of the population units will result in a variable rate of behavioral change

A central proposition of the dual SS model is that adaptation includes two processes with different learning rates (Fig. 5A) (*21*, *47*, *70*). However, within a single layer of the CPC model, an epiphenomenon of population coding is that units will appear to operate in different time scales even if the learning rate parameters are identical across all units (Fig. 5B). When an error is observed, cells with a preferred direction centered on this error will display relatively fast learning and quickly saturate (Fig. 5, C and D). In contrast, cells with a preferred direction slightly misaligned with the error direction will not only learn slower due to the weaker climbing fiber input but will also take longer to saturate. Hence, by the CPC model,

Table 1. Comparison of the CPC model and other models of sensorimotor adaptation. Summary of model performance on core phenomena. In evaluating each of the models, we used an implementation based on that presented in the associated paper.

	CPC	Dual state-space (*21*, *47*)	MoE (*67*)
Anterograde interference (Exp 2)	✓	✓	✗
Attenuation in relearning (Exp 3)	✓	✗	✗
No spontaneous recovery (Exp 3)	✓	✗	✓
Invariant to error consistency (Exp 4)	✓	✓	✗
Slower adaptation after variable perturbation (Exp 4)	✓	✗	✗
Fast single-trial learning after unpredictable perturbation (Exp 4/5/8)	✓	✓	✗
Different retention rates for variable and fixed perturbations (Exp 1/5)	✓	✓	✗
Minimal attenuation of the asymptote in half washout (Exp 6)	✓	✗	✗
Fast single-trial learning around the asymptote (Exp 6)	✓	✓	✗
Stable process is gated by the volatile process (Exps 7–8).	✓	✗	✗

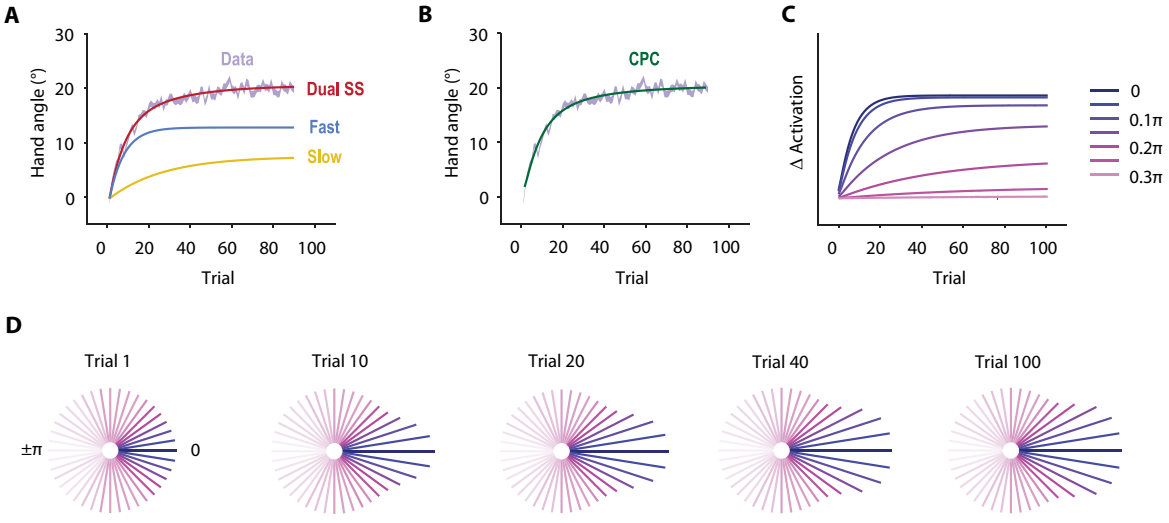

Fig. 5. Emergent variation in learning rate across the population units. (**A**) Learning curve from Tsay *et al.* in which participants were exposed to a 30° clamp. This function can be described as the sum of a fast process that contributes to the rapid change in hand angle early in learning and a slow process that continues to accumulate over time. The best-fitted dual SS model and the relative contribution of the fast and slow processes are shown. (**B**) The CPC model can account for learning function without positing different learning rates. (**C**) By the CPC model, the contribution from different units will vary over time due to their tuning for error direction. We mark the direction of the error as 0 in the unit tuning space. Cells tuned to error direction (i.e., 0) respond strongly, driving rapid early learning while saturating quickly. Cells with tuning slightly misaligned with the error direction (e.g., 0.2π) have a small error response but saturate slower; hence, they make a relatively large contribution late in training. (**D**) (C) plotted in polar space. Each vector corresponds to a cell with the orientation, indicating the cell's preferred error direction, and the length, indicating its activation strength.

the change in movement direction is determined by the collective activation of all units and thus can be regarded as a composite process of units with different learning trajectories arising from their error tuning.

Different retention rates in adaptation

We have shown the tuning features of cerebellar units, and their population dynamics within the CPC model explain a wide range of contextual effects in implicit adaptation, outperforming alternative models. While we used a two-layered model in these simulations, the predictions would also hold in a single-layered CPC model. However, the anatomy and physiology of the cerebellum suggest that plasticity effects in the cerebellar cortex and DCN can be quite distinct, perhaps constrained by different computational principles (*21*, *47*–*49*, *71*, *72*). We explore this issue in the following section: first, examining the evidence to suggest computational differences between the layers, and then testing predictions to ask how the layers interact with each other.

As shown above, experimental tasks that focus on learning rates are not ideal for assessing the existence and/or properties of different layers: A single-layered system can appear to be operating at multiple speeds. As an alternative, we used a variable perturbation task in which the sign and size of the perturbation were varied across trials (Exp 5). With this design, the forgetting rate of the system can be empirically measured as the ratio of the change of hand angle in response to the perturbation just experienced (1-back) relative to the previous perturbation (2-back; see Materials and Methods). Consistent with previous studies (*1*, *73*, *74*), we found prominent trial-by-trial adaptation in response to the random perturbations. Unexpectedly, the observed retention rate of 0.5 indicates that about half of the learning from the previous trial was forgotten over the 3-s intertrial interval (ITI) (Fig. 6, A and B). This low value stands in marked contrast with the empirically estimated retention rate from designs in which the perturbation is fixed (e.g., Exp 1, 0.98; Fig. 6C). When we run the same analysis on data from published studies using variable or fixed perturbations, we observed a similar marked difference in the retention rate (*18*, *74*–*77*).

This result could suggest that there are at least two adaptation processes with different retention rates (*47*, *72*). Alternatively, it might be taken to indicate the operation of a meta-learning process, where the forgetting rate is ramped up in response to a variable environment. To differentiate those two hypotheses, we ran an experiment (Exp 6) in which we first used a fixed perturbation for an extended block and then followed this with a half-washout phase in which 50% of the trials had no feedback and 50% had clamped feedback (Fig. 6D). There was a considerable drop in hand angle after each no-feedback trial, much larger than what would be predicted by a single-layered model parameterized with a retention rate estimated from a typical fixed design (Fig. 6E). The magnitude of those single-trial changes is comparable to what is observed in a variable design. A meta-learning model would attribute the drop in retention rate to the variable context (namely, the mixture of no-feedback and clamp trials). However, at odds with this hypothesis, the asymptote in the half-washout block largely persisted (Fig. 6D). Thus, the retention rate of the system appears to have remained fixed between the learning and half-washout blocks. Hence, the large trial-by-trial

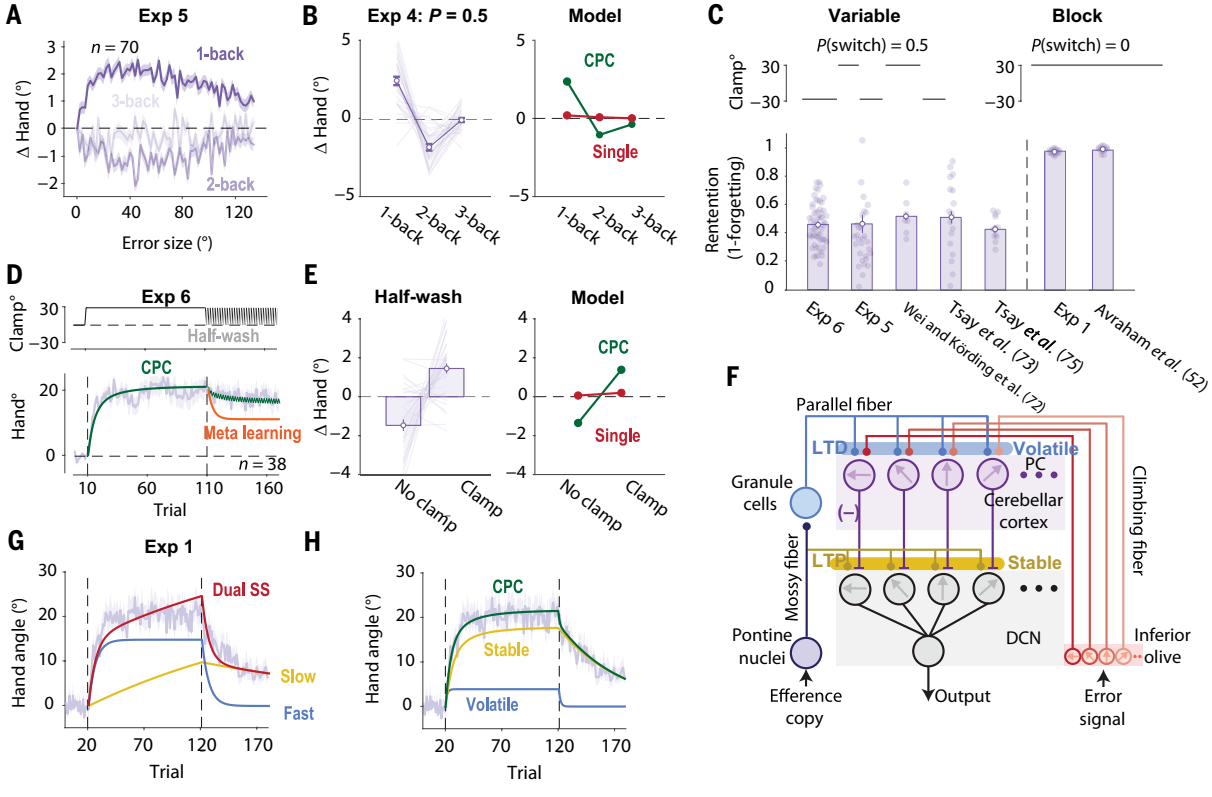

Fig. 6. Operation of volatile and stable processes in cerebellum-dependent adaptation. (**A**) Trial-by-trial change of hand angle (Δhand) as a function of the perturbation size on trial *n* − 1 (1-back), *n* − 2 (2-back), and *n* − 3 (3-back) in Exp 5. (**B**) Left: Similar analysis applied to the data from the variable phase of Exp 4 for the 50% switching condition. Right: The two-layer CPC model can account for the large yet transient change in hand angle observed in response to a random perturbation. A single-layered CPC model predicts negligible change due to its high retention rate measured from Exp 1. (**C**) Estimate of retention rate in experiments using variable or fixed perturbations. Reanalysis of data from Wei and Körding (*74*), Tsay *et al.* (Exp 2) (*75*), Tsay *et al.* (Exp 2) (*77*), and Avraham *et al.* (Exp 1) (*52*). All of the depicted experiments used a design with a single-target location. (**D**) In Exp 6, the half-washout phase entails a 50/50 mix of clamp and no-feedback trials. Consistent with the CPC model, only a small reduction in hand angle was observed during the half-washout phase, whereas the meta-learning model with a changeable retention rate predicts that the hand angle will be reduced by 40%. Purple functions indicate behavioral results. (**E**) Large trial-by-trial changes of the hand angle in the half-washout phase can only be predicted by the two-layered CPC model rather than a single-layered model. (**F**) The volatile process is hypothesized to produce LTD at the PF-PC synapse; the stable process is hypothesized to produce LTP at the MF-DCN synapse. (**G** and **H**) The dual-rate version of the CPC model (H) provides a better fit of the learning function in Exp 1 compared to the classic dual SS model (G).

changes in hand angle and a persistent asymptote are consistent with the dual-rate hypothesis.

Differential plasticity in the cerebellar cortex and DCN

Physiological studies have shown that learning in the DCN appears to be more stable compared to the cerebellar cortex. For example, learning-induced change in the firing rates of simple spikes in PCs may decrease after a few trials (*24*, *72*, *78*), whereas changes in the DCN typically last for days (*25*, *79*). Given the evidence reviewed in the previous section pointing to the existence of a system composed of units with distinct retention rates, we instantiated this difference in the two-layer CPC model such that plasticity within the cerebellar cortex/PC can produce changes that are weakly retained, whereas plasticity within the DCN is more persistent (Fig. 6F and fig. S3) (*80*, *81*).

This conjecture bears similarity to that proposed in previous dual-rate models (e.g., dual SS model) (*21*, *47*, *82*). However, there are substantial differences between these previous models and the two-layer CPC model in terms of how they characterize the dynamics of the two processes. A key feature of SS models is that adaptation reaches an asymptote when the trial-by-trial effects of learning and forgetting cancel each other out. However, it is difficult to simultaneously fit the acquisition and washout phases in response to a fixed perturbation with an SS model, even with the degrees of freedom conferred by a dual-rate variant (Fig. 6G). The CPC model provides an alternative account of asymptotic performance: We posit that there is a limit to neuroplasticity within the DCN units. The asymptote will primarily reflect this upper bound, given that these units have a high retention rate. There will also be a modest contribution from the PCs, given that these units have a low retention rate. Hence, the CPC model can readily fit the full learning and forgetting function in adaptation (Fig. 6H).

A stronger comparison of the two models is provided by the half-washout phase of Exp 6. The SS model predicts that during this phase, the asymptote will eventually drop to 50% of the original asymptote because learning occurs on just 50% of the trials, those with feedback (fig. S4). This prediction holds even in SS models that posit learning at multiple time scales (*21*, *63*). However, as noted above, the asymptote only showed a slight decrease when clamped feedback was presented on 50% of the trials, consistent with the predictions of the CPC model (fig. S4B).

A second difference from previous dual-rate models is that the CPC can account for the context effects discussed in Exps 2 to 4 (see Table 1). Moreover, by extending the dual coding feature in a two-layered system, the CPC model predicts a novel context effect in a random design experiment, one in which the sign of the perturbation is randomized: The trial-by-trial change in hand angle will decrease over the course of an experimental session even if the learning and retention rates of both layers are fixed. Early in the session, learning within both a volatile and stable layer will contribute to the change in performance. However, gradual changes will accumulate in units tuned to both directions within the stable layer, eventually reaching their asymptotic level of plasticity. Thus, late in the session, learning is essentially dependent solely on the rapid changes occurring within the volatile layer. The net effect is that the overall learning rate will decrease over the course of training (fig. S5, A and B), another example in which an apparent change in learning rate is emergent from the dynamics of the system. In contrast, the dual SS model predicts that the overall learning rate should be constant because only the fast process makes an observable response to random perturbations. The data are again consistent with the CPC model: The overall learning rate decreases over the course of a block of trials in which the size and direction of the perturbation are randomized (fig. S5C).

Learning within the DCN is gated by the cerebellar cortex

Given that the output of the PCs is the primary input to the DCN, we can ask how learning within the DCN is modulated by activity in the cerebellar cortex. By the CPC model, learning in the DCN is scaled by the change in simple spike activity of the PCs; in effect, the stable process is gated by the labile process (*49*). While this hierarchical organization has been proposed previously in the discussion of dual-rate models of adaptation (*47*), it has not been tested empirically.

One way to evaluate the gating hypothesis is to manipulate the duration of the ITI. The change in hand angle arising from a volatile process decreases with the passage of time. If the volatile process gates the stable process, then increasing the ITI should result in a much slower change in hand angle in a fixed design (Fig. 7B). In contrast, if the two processes operate in parallel (PARALLEL model), the operation of the stable process will not be influenced by variation in ITI. Higher asymptotic values in a short ITI condition would be solely due to the greater contribution of the volatile process.

To test this prediction, we used a variable design in Exp 7 using a 7-s ITI. We compared this long ITI condition with the data from Exp 4 in which the next trial started as soon as the hand was repositioned at the start location and thus had an ITI of 0 s (Fig. 7A). In this manner, we estimated the decay rate of the volatile process as a function of ITI. We then used the estimated parameter to predict the learning function in response to a fixed perturbation (Exp 8), comparing 7- and 0-s ITI conditions (Fig. 7C). To measure the learning rate of the stable process (DCN), we ignored the first five trials where there will be a substantial contribution from the volatile process and focused on trials 6 to 10.

The results were consistent with the predictions of the CPC model. Across these trials, the change in hand angle was much higher in the short ITI condition (Fig. 7C), consistent with the hypothesis that learning in the stable layer is modulated by the volatile layer. Moreover, the long ITI condition showed a slower decrease of hand angle compared to the short ITI condition in the initial washout trials (Fig. 7D). This suggests that the volatile process made a smaller contribution to learning in the long ITI condition. The difference in the forgetting rate diminished in late washout trials because the residual memory here comes from the state of the stable process.

We note that this version of the CPC model fails to capture one prominent feature in these data—the convergence of the two functions at the asymptote (Fig. 7F). The CPC model predicts that the advantage for the short ITI condition should persist, resulting in a lower asymptote in the long ITI condition. To address this issue, we consider a post hoc modification of the CPC model, adding an inhibitory connection from the DCN to the IO (Fig. 7G) consistent with physiological studies (*83*–*85*). The inhibitory signal to IO will reduce its input strength to the cerebellar cortex and thus decrease the number of PCs that generate CSs (*86*). We posit that the effects of this inhibition will be strengthened when the input re-occurs over a short interval. Hence, more learning units can be recruited in the long ITI condition, although plasticity within each unit is reduced because of the memory decay that occurs during the long ITI

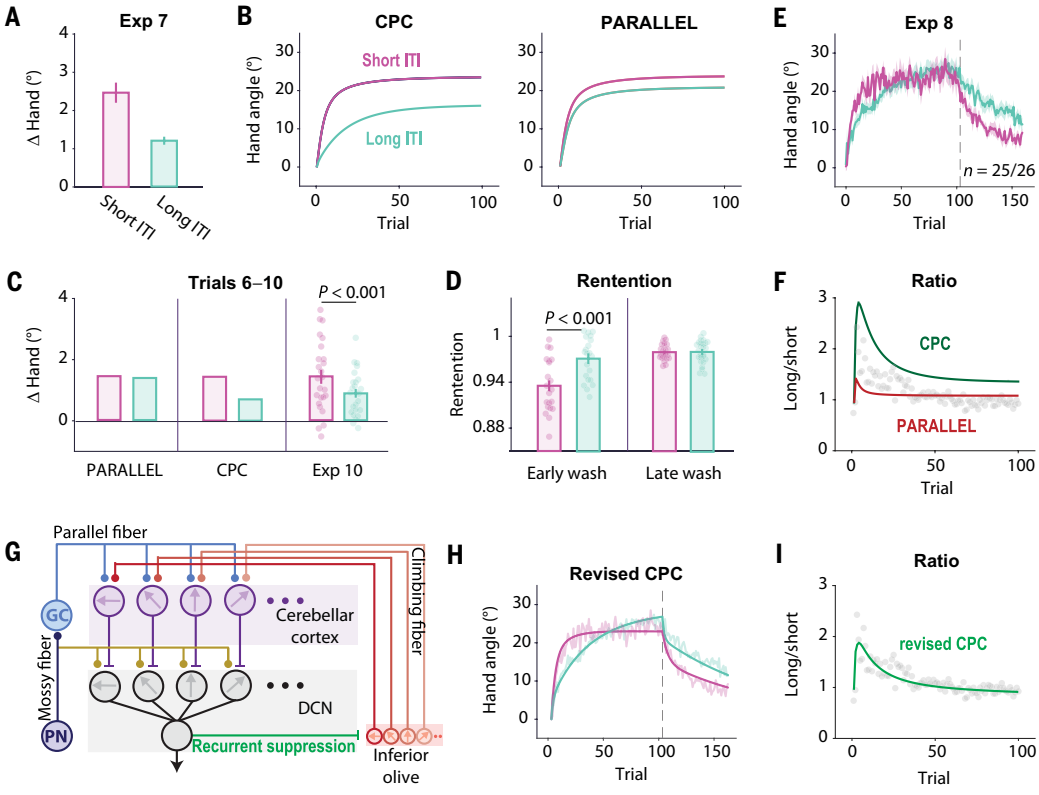

Fig. 7. The stable process is gated by the volatile process. (**A**) Trial-by-trial change in response to a variable perturbation with a short (data taken from Exp 4; *P*(switch) = 0.5 condition) or long ITI (Exp 7). (**B**) Predictions of learning functions under the gating assumption of the CPC model and the alternative model in which the two processes operate independently (PARALLEL). The differences between the two functions are reduced over time. However, inconsistent with either model, the learning curve in the two conditions reached a common asymptote. (**C**) Model predictions and results from Exp 8 for the change of hand angle across trials 5 to 10. The change of hand angle is higher in the short ITI condition. (**D**) The retention rate is larger in the initial no-feedback trials in the long ITI condition because the volatile process is weakened by the passage of time. However, the retention rate is similar across the two ITI conditions late in washout, consistent with the hypothesis that only the stable process remains operative. (**E**) Learning functions in Exp 8 using either a short or long ITI. (**F**) Hand angle ratio between the short ITI and the long ITI conditions deviates from predictions of both models. The ratio falls between the two model predictions early in training and is smaller than predicted by both models late in training. (**G**) Th revised CPC model includes inhibitory projection from DCN to the IO. This suppresses the error signal conveyed by the climbing fibers. This suppression is assumed to decay with time, becoming negligible in the long ITI condition in the revised CPC model. PN, pontine nuclei; GC, granule cell. (**H** and **I**) Predictions of the revised CPC model provide a good fit to the learning curve (H) and the change in the ratio between the long and short ITI conditions (I) in Exp 8. The shaded area and error bar indicate standard error.

(fig. S6). The revised CPC generates learning functions that provide good fits in both ITI conditions (Fig. 7, H and I). After reestimating all of the parameters using this variant of the CPC, we observed negligible effects on the predictions reported for the other experiments (fig. S7). In sum, these results point to a hierarchical arrangement in which the volatile process gates the operation of the stable process.

The revised two-layer CPC model can account for another classic learning effect, contextual interference, referring to the phenomenon in which performance gains are slower when training involves multiple contexts (e.g., reaching toward multiple directions) compared to training in a single context, but retention is better in the former (*87*, *88*). This phenomenon, at least in the context of implicit adaptation, is an emergent property of the parallel operation of volatile and stable learning processes (see result S2).

DISCUSSION

To support flexible behavior, an organism needs to choose an action appropriate for a given context and execute a movement to achieve the desired outcome. A large body of work has sought to delineate the principles of these learning processes, with one prominent question centering on how the processes incorporate context and respond to uncertainty. Here, we address this question with respect to the cerebellum, a subcortical structure long recognized as essential for keeping the sensorimotor system precisely calibrated in the face of fluctuations in the environment or state of the agent. We developed a population-coding model incorporating two key features: (i) Units are tuned to both movement direction and error direction, and (ii) learning occurs at different rates in the cerebellar cortex and DCN, with the former characterized by a fast, volatile process and the latter characterized by a slower, stable process. Our CPC model provides a parsimonious account of a diverse range of learning phenomena and offers insight into the temporal dynamics of learning (table S1). Moreover, the CPC model offers specific predictions about computations within the cerebellar circuit that are amenable to testing in future neurophysiological studies.

Context dependency as an emergent property of population coding

There is no explicit role of context in the CPC model in the sense that a context does not trigger the retrieval of its associated response. Rather, the signatures of context-dependent learning and environmental

uncertainty emerge naturally from a population of tuned elements that operate in an inflexible manner. In this way, the CPC model diverges from classic models in how it accounts for the operation of the system when a previously encountered context is reexperienced. Under such circumstances, classic models predict savings in relearning, given that the context facilitates the retrieval of the appropriate response (*21*, *67*). In contrast, the CPC model accounts for the fact that implicit adaptation not only fails to show savings but actually can also show attenuation (*18*). This attenuation can be seen as another manifestation of anterograde interference: Because of the tuning properties of neurons in the cerebellar cortex and DCN, persistent activation in response to error in one direction will interfere with the response to an error in a different direction.

Our results indicate that many contextual effects observed in sensorimotor adaptation tasks are likely due to the operation of other learning processes. In particular, savings and spontaneous recovery are likely due to the rapid recall of an aiming strategy that had previously proven successful (*18*, *65*). The current work adds to the body of literature highlighting the importance of identifying the unique computational principles associated with different learning processes. For example, the COIN model assumes that COIN is relevant for both explicit and implicit processes. The current empirical and theoretical results suggest that this assumption may only be relevant for the explicit system.

Given the impressive flexibility in human motor learning, it might be surprising that implicit adaptation does not explicitly track the context or uncertainty of the environment (*31*, *59*, *89*). We propose that this rigidity reflects a degree of modularity between processes associated with action selection and those related to movement implementation. The cerebellum is part of a system designed to use error information to ensure the accurate execution of a planned movement. The emphasis here is on "planned movement" rather than "desired outcome" to underscore the point that this system appears to operate independently of the task goal; participants will adapt to sensory prediction errors even when the change in behavior is detrimental to task success (*1*, *12*). This modularity provides a means to keep the system properly calibrated across changes in the internal state of the organism (e.g., perceptual biases and fatigue), factors that do not require a change in action planning. In contrast, other learning systems are designed to use error information related to task success to determine whether the selected action was optimal given the current context. These systems would be optimized to track contextual shifts in determining the appropriate policy. Consistent with this hypothesis, contextual effects such as savings and sensitivity to uncertainty are observed in adaptation tasks that benefit from changes in action selection (*67*, *90*, *91*).

We have focused here on showing how implicit adaptation does not infer context from the error history; rather, contextual-like modulations arise from the population activation of a cerebellar-like network. However, many studies have demonstrated other ways in which context influences sensorimotor adaptation. Spatial generalization provides one example where implicit adaptation at one location shows limited transfer to other locations (*1*, *64*, *92*). There is also a large body of work showing how environmental cues can serve to distinguish different memories. For example, variation in the start or terminal position (*61*, *93*) or variation in the movement initiation cues (*52*, *62*, *94*) can serve to distinguish between different perturbations.

The emphasis on population activity offers a relatively direct way to modify the CPC model to account for these contextual modulations. Each PC receives two distinct inputs: climbing fibers and PFs. For this paper, we mainly focused on the former, with error tuning constrained by the climbing fiber input. The PF input conveys contextual information, including the state of the body, the location of the target, and the environment. Assuming functional units in the cerebellar cortex are organized by their PF input, generalization and representational segregation will be determined by the degree of overlap between the inputs. Consider spatial generalization: For a given target position, activation will be strongest in units tuned to that position and fall off according to a generalization function. With this architecture, training at one target direction will produce implicit adaptation for reaches to nearby target locations but show limited adaptation to far locations. A similar principle can be applied to explain the contextual effects observed when environmental cues are manipulated. Presumably, the population activity of the cerebellar units is also modulated by the PF inputs that convey information about variables such as the start position or cues associated with different perturbations. We formalize this idea in result S1.

Hierarchical organization within the cerebellum for implicit adaptation

The behavior observed in adaptation studies is assumed to reflect the function of learning processes that operate at different time scales (*21*, *82*). It has been suggested that fast and slow processes correspond to explicit and implicit learning processes (*63*). Using variable and fixed designs, we provide evidence that learning limited to just the implicit system operates at different timescales, a notion similar to the original framing of the dual SS model (*21*, *47*). However, rather than view these as processes that operate in parallel, our empirical and modeling results highlight a hierarchical organization in which accumulated learning from a volatile process will constrain the learning rate of a stable process. This organization readily maps onto a two-layered network formed by the cerebellar cortex and DCN, with the output from the former gating learning within the latter. The neurophysiological evidence is consistent with this assumption. While the change of SS activation in the PCs can happen within a few trials (*22*, *24*), changes within the DCN can maintain learning across days (*25*, *79*). Reflective of the hierarchical organization, we showed that there is an asymmetric dependency such that the synaptic strength in the cerebellar cortex determines the PC output that modulates learning within the DCN.

We recognize that a two-layered model is a simplification. To explain the asymptotic convergence in the long and short ITI conditions, we had to incorporate a third layer into the model, creating a closed loop by adding a projection from the DCN to the IO. While the anatomy supports the existence of this pathway, to achieve convergence, we added two specific features to the dynamics of this pathway. First, the intensity of the inhibition from the DCN to the IO exhibits an intensity decrease over time (*95*, *96*). Second, the projection is generic, inhibiting IO units independent of the directional tuning of the DCN neuron. These two assumptions need to be tested in future physiological studies.

We note that an anatomical feature of the cerebellum is the high convergence of PCs onto the DCN (*97*). Given our assumption that learning in the PC layer is volatile, this convergence would provide a population-level mechanism to reduce noise and thus send an

accurate teaching signal to the DCN. In our current simulation, we did not include noise or redundant units in the PC layer. However, the model predictions would be unchanged if we incorporated noise and expanded the PC layer to include duplicate units for each direction, assuming that these converge to the same DCN unit.

Another simplification of the model is the restriction of LTD and LTP in the PC layer and DCN layer, respectively. Our assumptions regarding the locus of LTD and LTP are not critical in terms of the performance of the model. The results would be similar if we assumed the reverse organization or had a mixture of LTD and LTP at each layer. A more realistic model should incorporate some degree of bidirectionality, given that LTP is also observed in the PC layer (*39*, *78*). Whereas we focused on a passive forgetting process, LTP in the PC layer has been postulated to play a role in an active unlearning process that produces extinction (*85*, *98*). In this model, learning in the PCs and DCN results in the DCN output that suppresses IO activation. Because of this suppression, the CS rate will be lower than baseline when the error is removed, thereby inducing LTP in the PC layer and resulting in unlearning. Thus, in addition to LTD, this model allows for LTP in the PC layer, which offers a different interpretation of forgetting. Computationally, the forgetting parameter would be replaced by a rate of LTP in the PC layer, and the predictions of the model will be largely unchanged.

Although our model focuses on the cerebellum and sensorimotor learning, the core computational principles may offer insight into how the nervous system responds to environmental uncertainty. The population-coding aspect of the CPC model is similar to models of perceptual learning that include a basis set of tuned elements (*99*). For example, in models of time perception, contextual effects on perceived duration have been proposed to reflect the interaction of units tuned to different durations (*100*, *101*). Applied to this domain, the CPC model could be used to derive specific predictions of how temporal perception is modulated by uncertainty and establish boundary conditions for interference. Moreover, the two-layered network in the CPC model provides a powerful framework to understand how learning can involve multiple processes that follow different temporal dynamics, a phenomenon widely observed in cognitive tasks. For instance, value learning has been hypothesized to reflect the joint operation of a fast, volatile process and a slow, stable process (*88*). While these processes are typically viewed as operating in parallel, the CPC model offers an example of how a hierarchical framework might prove more parsimonious.

MATERIALS AND METHODS

CPC model

Here, we extend the classic Marr-Albus model, focusing on how learning is modulated when the environment is variable. A foundational idea for our model is inspired by a recent work showing how PCs in the oculomotor cerebellar cortex are simultaneously tuned to both movement direction and the error that is associated with that movement (*22*, *39*).

To examine the implications of these tuning properties for cerebellar-dependent learning, we incorporate PC tuning into a learning model. Specifically, we formalize the teaching signal, the CS activity of a PC with a preferred direction of $i (0 \le i < \pi)$ in response to a movement error e (Fig. 1D) as

$$CS_i^n = \mathrm{VM}\left(\theta^e, i, s\right) F(\rho^e) \tag{1}$$

where $\mathrm{VM}(i, s)$ is the probability density function of a simplified circular (von Mises) distribution with a mean of i and SD of s. θ^e and ρ^e refer to the direction and the size of e, respectively, and n is the trial number. Given that we only applied one error size across all experiments, $F(\rho^e)$ is not relevant and set as 1 here (*74*, *76*). The form of this nonlinear relationship is not relevant in the experiments with a fixed perturbation; for those experiments, the exponent was set to 1.

Following the Marr-Albus model, the occurrence of a CS suppresses the strength of the PF input synapse (w) through LTD

$$w_i^{n+1} = -lCS_i^n + f\left(w_o - w_i^n\right) + w_i^n \tag{2}$$

where l ($l > 0$) and f ($0 < f < 1$) are the learning and forgetting rates, respectively and w_o is the baseline synaptic strength. Because the level of single-spike (SS) activity will be greatest for cells coding a movement direction opposite to the error, the modulation of synaptic strength will drive the next movement in a direction that corrects for the observed error.

The preceding paragraph describes how PF synapses onto PCs are modified. A second prominent site of plasticity is at DCN (*25*, *79*). PC and DCN neurons are organized such that they share the same tuning direction for movement (*48*). We posit that learning at the DCN is gated by learning at the cerebellar cortex. Specifically, LTD at PF-PC synapses will reduce inhibitory PC input to the DCN, resulting in LTP at the MF-DCN synapses (m) (Fig. 1E)

$$m_i^{n+1} = \left(w_o - w_i^n\right)ß\left(m_{\max} - m_i^n\right) + \alpha\left(m_o - m_i^n\right) + m_i^n \tag{3}$$

where ß and α are the learning rate and the forgetting rate of the DCN input synapse, respectively. The parameters m_o and $m_{\max}$ represent baseline and maximal synaptic strength, respectively, and were arbitrarily set as 0.15 and 1. The latter constraint is based on empirical results, showing that implicit adaptation saturates independent of the error size. Although physiological studies have shown that PC input is essential for plasticity at MF-DCN synapses (*102*–*104*), how this plasticity is modulated by the level of PC activity is unclear. Hence, further empirical studies are needed to evaluate the assumption that decreasing PC activity will facilitate LTP at MF-DCN synapses.

In this initial version of the CPC model, we assumed that the PC layer is dominated by LTD, and the DCN layer is dominated by LTP. Classically, PC-layer learning has emphasized LTD (*4*, *5*, *105*, *106*), including recent evidence from rodent work showing LTD during upper limb reach adaptation (*6*). There is a dearth of evidence concerning the mechanisms of learning in the DCN. Hence, we assumed that learning here follows a simple Hebbian process, one consistent with LTP.

Considering the two sites of plasticity, DCN activity on a repeated trial following a movement error can be formalized as

$$DCN_i^{n+1} = m_i^{n+1} - \gamma\, w_i^{n+1} \tag{4}$$

where γ is a scaling factor. The output of the population of DCN neurons will correspond to the change in movement direction in response to an error, a signal that can be used to adjust the movement. This can be expressed as (Fig. 1F)

$$\boldsymbol{h}^{n+1} = -\varepsilon \sum_i \boldsymbol{v}_i \mathrm{DCN}_i^{n+1} \tag{5}$$

where $\boldsymbol{h}^n$ is a vector representing the hand angle on trial n, $\boldsymbol{v}_i$ is a vector representing the tuning direction of unit i, and ε is a scaling factor to transfer the neural activity into hand angle.

To help clarify the importance of a two-layer model, we describe two variants of the CPC model. First, we implemented a single-layer version of the CPC model by modifying Eq. 4 to

$$DCN_i^{n+1} = m_i^{n+1} \quad (6)$$

In this version, the output of the system is solely determined by the strength of the MF-DCN. We note that we do not specify, for the purposes of this paper, whether the cerebellum is best viewed as a forward or inverse model. The current implementation of the CPC model most resembles an inverse model, given that the system modifies the motor commands based on the error. However, the model could be reframed as a forward model with the output a prediction that is fed into an (cerebellar or extracerebellar) inverse model that refines the motor commands.

Parameterization of the CPC model

In our simulations of PC and DCN neurons, we modeled 1000 units for each layer and set the SD of the tuning function (s) to 0.2π. The results of most simulations were not sensitive to these two parameters. While anatomical studies show considerable convergence from the PC layer to the DCN, for simplicity, we opted to impose a one-to-one connection between the PC and DCN.

We used an empirical approach to estimate the learning rate (l) and forgetting rate (f) for PF-PC synapses, using the data from Exp 4 in which ±30° clamps were presented with a 50% switching probability. To measure single-trial learning, we calculate the change of hand angle between trial n and trial $n-1$, flipping the sign when the clamp on trial $n-1$ was negative. To measure single-trial forgetting, we calculate the change of hand angle between trial n and trial $n-1$, flipping the sign when the clamp on trial $n-2$ was negative.

PF-PC forgetting (f) is the ratio of single-trial forgetting and single-trial learning. By definition, retention rate is $1-(f)$. We applied the same method to measure the retention for all variable designs, and this gave us an f around 0.5. Model simulations indicate that this method can precisely estimate retention when the perturbation is random. In all of the analyses, we excluded the first 50 trials because learning at this early stage is influenced by both PC and DCN. For comparing the learning rate between early and late training in a by variable design, we used the same general approach but limited the analysis to the first 50 trials to estimate early learning (fig. S7).

The baseline and maximal strength of MF-DCN synapses can be set to arbitrary values: We used 1 and 1.85 for m_o and m_{max}, respectively. We measured the retention rate of the MF-DCN synapse (α) empirically using the data from the no-feedback washout phase in Exp 1

$$\alpha = \sqrt[10]{\text{mean}\left(\frac{y^{n+10}}{y^n}\right)} \quad (7)$$

where y^n is the hand angle in trial n. The first 20 trials in the washout phase were excluded because they may be contaminated by a volatile process.

The learning rate of DCN (ß) and the scaling factors (γ, ε) were jointly fitted from the learning block in Exp 1. This results in a set of parameters: $l = 2, f = 0.5$, ß = 0.05, α = 0.018, γ = 0.15, and ε = 130. These parameters were fixed in the simulations of all the other experiments. The only exception is Exp 8, where we set the PF-PC retention rate for the long ITI conditions (f') to be 0.3, based on the empirically observed value in the variable design of Exp 7.

Revised CPC model

The results of Exp 7 led us to develop a post hoc variant in which the output of the cerebellum modulates the input, an idea that is consistent with cerebellar anatomy and physiology (*83*, *107*). The basic version of the CPC model predicts that learning in a long ITI condition will reach a lower asymptote compared to a short ITI condition. This occurs because the contribution of the volatile process is suppressed in the long ITI condition. However, the results of Exp 8 showed that, with a sufficient number of trials, learning in the long ITI condition eventually reaches the same asymptote as in the short ITI condition. This observation led us to revise the model by adding an inhibitory pathway from the DCN to the IO (*83*, *107*).

We assume that the output of the DCN integrates the activation of directionally tuned units and that this signal serves as a generic inhibitory signal to the IO. We implemented this generic suppression by subtracting a common value from the activation of cells tuned to all error directions in the IO

$$IO_i = 1 - \omega * \sum\nolimits_i DCN_i^n \quad (8)$$

$$\text{if } IO_i > 0: cs_i' = IO_i * cs_i \text{ otherwise: } cs_i' = 0 \quad (9)$$

where ω represents the strength of suppression. Given the assumption that ω decreases across time, we used separate parameter values of ω for the long and short ITI conditions, and $\sum_i DCN_i^n$ is the sum of the change of all DCN units relative to their baseline activities. cs_i' is the corrected CS activation value after taking the DCN-IO pathway into consideration and replaces the cs_i term in Eqs. 1 to 5. The retention rates of the stable processes (α = 0.012) in the revised CPC model were set as in the basic model. The forgetting rate of labile process was empirically measured from Exp 4 and Exp 7: $f(\text{short}) = 0.5$; $f(\text{long}) = 0.75$. The other parameters (l, ß, ε, γ, ω) were jointly fitted from two data sets: the learning block in Exp 1 and Exp 7: $l = 1.3$, ß = 0.1, α = 0.012, γ = 0.52, ε = 202, ω(short) = 2.8, and ω(long) = 0.

We also simulated the revised CPC model to explain the results in Tsay *et al.* (*87*) in which learning was slower when reaches were directed to three targets spaced by 120° compared to when the reaches were to a single target, but the two conditions reached a similar asymptote. The CPC model will treat each target independently. The following parameters were applied: $l = 0.98, f = 0.5$, ß = 0.1, α = 0.018, γ = 0.4, and ε = 190. In addition, ω was set to 2.5 for the single-target condition and 0 for the three-target condition. These values are consistent with those applied for the short- and long-ITI conditions in Exp 8.

Alternative models

Dual SS model

We used a standard version of an SS model (*21*, *108*)

$$x(n+1) = a * x(n) + b(e,n)e(n) + \varepsilon_x(n) \quad (10)$$

where x is the internal estimate of the motor state (i.e., the hand movement required to compensate for the perturbation), a is the

retention factor, $e(n)$ is the size of the perturbation in trial n, b is the error sensitivity for a given error size, and ε_x represents planning noise.

The actual motor response on trial n is given as

$$y(n) = x(n) + \varepsilon_y(n) \tag{11}$$

where y is the reaching direction relative to the target, determined by $x(n)$ and motor noise, ε_y.

The observation of spontaneous recovery in classic sensorimotor adaptation tasks led to an expanded version of the SS model, one in which learning mechanisms were hypothesized to operate at multiple rates (*21*, *108*). Here, we used a dual SS model, adding a second, slower learning process (xs) with a different retention rate (as) and learning rate (bs)

$$xs(n+1) = as * xs(n) + bs(e,n)e(n) + \varepsilon_{xs}(n) \tag{12}$$

Where $as > a$ and $bs < b$. Hence, Eq. 11 can be written as

$$y(n) = x(n) + xs(n) + \varepsilon_y(n) \tag{13}$$

MoE model

The MoE model describes how the learning rate in the SS model is modulated by experience. In the MoE model, error sensitivity (b) is set to an initial value that is modulated by errors that are experienced during training. Specifically, $b(e,n)$ will increase if the error on trial $n + 1$ shares the same sign, and $b(e, n)$ will decrease if the error on trial $n + 1$ is of the opposite sign. This is formalized as

$$\begin{aligned} b[e(n), n+1] &= c * \{b[e(n), n+1] - b0\} \\ &+ b0 + d * \text{sign}[e(n) * e(n+1)] \end{aligned} \tag{14}$$

where c and d are the learning rate and retention rate of b, respectively. Because the error size is fixed at 30° in our experiments, we replace $b(e)$ with a single value b. $b0$ represents the baseline error sensitivity.

COIN model

We simulated the COIN using the code provided by Heald *et al.* (*31*), focusing on how the model accounts for savings and spontaneous recovery in visuomotor rotation tasks. Central to the model is the assumption that participants make an inference about the context and its associated perturbation from the visual feedback and reach angle. However, in the clamp task, the feedback is not contingent on the reach angle. Given this, we considered how we might simulate the COIN model in a clamp task. First, we might assume that, given the instruction to ignore the feedback, the system makes no inference from the clamp feedback and thus generates no adaptation. Second, the system might treat the feedback as if it were contingent feedback. However, because the change in reach angle does not reduce the error, the inferred perturbation size would be unbounded (may go to infinity).

Given that the COIN model cannot be applied to simulate the clamp task, we opted to simulate the model with a standard visuomotor rotation task to illustrate how contextual effects, such as savings and spontaneous recovery, are generated when both implicit and explicit processes contribute to learning. These simulations are not for direct model comparison but can be compared to the behavioral results observed in the experiment in which we examine these contextual effects under conditions in which learning is purely implicit.

We note that the basic COIN model does not distinguish between implicit and explicit learning processes. The authors describe a variant of COIN in which they include a bias term to model the implicit component, inferred from the discrepancy between visual and proprioceptive inputs. In this variant, the state term now refers only to the explicit component to infer the perturbation (*31*). COIN is applied to both the implicit and explicit components. However, this version of COIN is also not suited for making meaningful predictions with clamped feedback given the two issues discussed above. Hence, we limited our simulation of COIN to the basic model in standard visuomotor rotation tasks.

Behavioral experiments

Participants

A total of 451 participants (297 female, mean age = 28.0, SD = 5.3) was recruited through the website prolific.co. Across and within experiments, random assignment to conditions and blinding was achieved through online recruitment and automated execution of the experimental protocols. Participants were naïve to the purpose of the experiments. The typical sample size for adaptation tasks such as those reported in this paper is 10 to 20 participants per group. Here, we recruited ~30 participants per group, given that online data can be noisier (*77*, *109*). After eliminating participants who failed to meet our performance criteria (2.8%; see below), the analyses were based on data from 438 participants. On the basis of a survey included in a prescreening questionnaire, the participants were right handed with normal or corrected-to-normal vision. The participants were paid on the basis of a rate of $8/hour. The protocol was approved by the Institutional Review Board at the University of California, Berkeley (approval number: 2016-02-8439). Informed consent was obtained from all participants.

Apparatus

All of the behavioral experiments were conducted online using a website-based experimental platform, OnPoint (*77*), which was written in JavaScript and presented via Google Chrome. It was designed to operate on any laptop computer. Visual stimuli were presented on the laptop monitor, and movements were produced on the computer trackpad. Data were collected and stored using Google Firebase.

Clamp rotation task

We applied clamp feedback in the experiments, under the assumption that learning in response to this type of feedback is limited to implicit, cerebellar-dependent sensorimotor recalibration. To start each trial, the participant moved the cursor to a white start circle (radius: 1% of the screen height) positioned in the center of the screen. After 500 ms, the target, a blue circle (radius: 1% of the screen height), appeared with the radial distance set to 40% of the screen size. The target appeared at −45°, a workspace location selected because it exhibits minimal bias across participants (*110*). The participant was instructed to produce a rapid, out-and-back movement, attempting to intersect the target. If the movement time (from onset to time at which movement amplitude reached the target) was longer than 500 ms, then the message "too slow" was presented on the screen for 500 ms.

There were three types of feedback. On veridical feedback trials, the position of the cursor moved was matched to the position of the hand, subject to the translation in reference frames (screen assumed to be vertical and hand movement assumed to be horizontal) and scaling (trackpad space expanded to encompass most of the screen). On clamped feedback trials, the cursor followed a fixed path. As with veridical feedback, the radial location of the cursor was based on the radial extent of the participant's hand. However, the angular

position of the cursor was independent of the position of the hand and was instead determined relative to the position of the target. The clamp angle was set at 30° relative to the target except for Exps 5 and 8 (see below). On no-feedback trials, the cursor was blanked at movement onset.

On veridical and clamped feedback trials, after the amplitude of the movement reached the target distance, the cursor was presented at the target distance for another 50 ms, and then it disappeared. The target disappeared after 200 ms. The cursor was then reset to a random position on an invisible circle with a radius equal to 10% of the target distance, and the participant moved the cursor back to the start circle.

At the onset of the first block of trials involving perturbed feedback, the experiment was paused, and a set of instructions was presented to describe the clamped feedback. The participant was informed that the cursor would no longer be linked to their movement but rather would follow a fixed path on all trials. The participant was instructed to always reach directly to the target, ignoring the cursor. These instructions were then repeated twice to emphasize the atypical nature of the feedback. After the first 10 trials with clamped feedback, a new instruction screen appeared in which the participant was asked to indicate where they were aiming on each trial. If the participant indicated that they were reaching somewhere other than the target, then the experiment was terminated.

Each experiment started with two baseline blocks: first, a no-feedback block of 10 trials and, second, a veridical feedback block of 10 trials. For experiments using a fixed design (direction and size of perturbation remain constant), the direction of the clamp (counterclockwise and clockwise) was counterbalanced across participants.

Experiment 1

Exp 1 was designed to determine the parameters of the CPC model. There was a total of 180 trials. The two baseline blocks were followed by a learning block of 100 trials with clamped feedback with learning expected to reach an asymptotic level in response to a fixed perturbation. This was followed by a final no-feedback block of 60 trials. Thirty participants were recruited for Exp 1 (29 valid; five males, age: 27.4 ± 4.9 years).

Experiment 2

Exp 2 was designed to measure anterograde interference. The baseline and initial perturbation blocks were as in Exp 1. For the final block (150 trials), the direction of the clamp was reversed (e.g., from 30° to −30°). Thirty participants were recruited for Exp 2 (30 valid; 10 males, age: 30.3 ± 4.3 years).

Experiment 3

Exp 3 was designed to assess spontaneous recovery and savings in implicit adaptation. The baseline and initial perturbation blocks were as in Exp 2. We then included a 15-trial block with the clamp reversed under the assumption that this would be a sufficient number of trials to bring the hand angle back to the baseline. This was followed by no-feedback block (35 trials) to examine spontaneous recovery and then a 100-trial relearning block in which the clamp feedback was identical to that used in the first perturbation block. Thirty-four participants were recruited for Exp 3 (34 valid; 16 males, age: 22.7 ± 4.8 years).

Experiment 4

Exp 4 examined how the consistency of the perturbation influenced implicit adaptation. The first blocks were identical to Exp 3, providing initial exposure to clamped feedback and then a reversed clamp to bring the hand angle back to baseline. This was followed by a 300-trial block in which the clamp changed sign in a probabilistic manner. The probability of a sign change was 90, 50, and 12.5% in a between-subject manipulation. The sequence of clamps was preset to ensure that clockwise and counterclockwise occurred on 50% of the trials each across the 300 trials. The experiment ended with a relearning block in which the initial perturbation was presented for 100 trials. A total of 36, 40, and 36 participants were recruited for 90, 50, and 12.5% conditions, respectively (34, 38, and 33 valid; 37 males, age: 28.6 ± 5.5 years).

Experiment 5

To estimate the learning rate and retention at the top layer of the CPC model, the PF-PC synapse, we used a variable design in which the error size and direction varied across trials. After the two baseline sections, participants completed a 540-trial random perturbation block. Here, the clamp size ranged from −135° to 135° in steps of 1°. The size and direction were determined at random with the constraint that each clamp was selected once every 270 trials. Seventy-two participants were recruited for Exp 5 (70 valid; 25 males, age: 26.2 ± 5.2 years).

Experiment 6

Exp 6 was designed to evaluate different models of asymptotic adaptation. A 10-trial feedback baseline block was followed by a learning block of 100 trials with clamped feedback. We then alternated between no-feedback and clamp-feedback trials for 60 trials (half-wash phase). Forty participants were recruited for Exp 6 (38 valid; eight males, age: 30.7 ± 6.6 years).

Experiment 7

To quantify the temporal dynamics of volatile processes, we used variable clamped feedback with extended ITI in Exp 7. For the long ITI, the interval between the end of one trial and the start of the next trial was 6, 7, or 8 s, randomized across trials. The message "wait" was displayed on the monitor after each trial. Exp 7 included two baseline blocks and a 180-trial learning block in which a 30° perturbation was randomly selected to be either clockwise or counterclockwise, subject to the constraint that each direction occurred four times every eight trials. For the short ITI condition, we used the data from Exp 4 for the variable condition (0-s ITI). Twenty-eight participants were recruited for each condition (27 valid; 13 males, age: 28.1 ± 4.8 years).

Experiment 8

To understand how the volatile and stable learning processes are jointly modulated by time, we used a fixed design in Exp 8. The design was similar to that used in Exp 1 with one notable modification. We included a 10-trial familiarization block following the two baseline blocks to demonstrate the clamp feedback. The clamp size in the familiarization block varied from −90° to 90° across trials to show that the cursor is unaffected by the direction of hand movement. To avoid the influence of preexposure to the error signal on learning, the familiarization block used a different target (45°) from the other blocks (315°). Two groups of participants performed the task with either long ITI (6 to 8 s) or short ITI (0 s). Twenty-six participants were recruited for each condition (51 valid; 21 males, age: 26.8 ± 4.6 years).

Data analyses

Hand angle was calculated as the angle difference between a line from the start position to the target and a line from the start position to the hand position at the target radius. Positive values indicate hand angles in the opposite direction of the perturbation, the direction

one would expect because of adaptation. Trials with a movement duration longer than 500 ms or an error larger than 70° were excluded from the analyses. We excluded the entire data from participants who had less than 70% valid trials (2.8% participants). Between-condition comparisons were performed with *t* tests or analysis of variances (ANOVAs). Learning and relearning were compared by a paired *t* test. For all the statistical tests, we confirmed that the data met the assumptions of a Gaussian distribution and homoscedasticity.

Supplementary Materials

This PDF file includes:

Supplementary Text
Figs. S1 to S9

REFERENCES AND NOTES

1. J. R. Morehead, J. A. Taylor, D. E. Parvin, R. B. Ivry, Characteristics of implicit sensorimotor adaptation revealed by task-irrelevant clamped feedback. *J. Cogn. Neurosci.* **29**, 1061–1074 (2017).
2. J. A. Taylor, N. M. Klemfuss, R. B. Ivry, An explicit strategy prevails when the cerebellum fails to compute movement errors. *Cerebellum* **9**, 580–586 (2010).
3. J. A. Taylor, R. B. Ivry, Cerebellar and prefrontal cortex contributions to adaptation, strategies, and reinforcement learning. *Prog. Brain Res.* **210**, 217–253 (2014).
4. M. Ito, Mechanisms of motor learning in the cerebellum. *Brain Res.* **886**, 237–245 (2000).
5. J. S. Albus, A theory of cerebellar function. *Math. Biosci.* **10**, 25–61 (1971).
6. D. J. Calame, M. I. Becker, A. L. Person, Cerebellar associative learning underlies skilled reach adaptation. *Nat. Neurosci.* **26**, 1068–1079 (2023).
7. C. Albergaria, N. T. Silva, D. L. Pritchett, M. R. Carey, Locomotor activity modulates associative learning in mouse cerebellum. *Nat. Neurosci.* **21**, 725–735 (2018).
8. C. H. Yeo, M. J. Hardiman, M. Glickstein, Classical conditioning of the nictitating membrane response of the rabbit. I. Lesions of the cerebellar nuclei. *Exp. Brain Res.* **60**, 87–98 (1985).
9. A. J. Bastian, Moving, sensing and learning with cerebellar damage. *Curr. Opin. Neurobiol.* **21**, 596–601 (2011).
10. M. Kawato, Internal models for motor control and trajectory planning. *Curr. Opin. Neurobiol.* **9**, 718–727 (1999).
11. T. J. Ebner, S. Pasalar, Cerebellum predicts the future motor state. *Cerebellum* **7**, 583–588 (2008).
12. P. Mazzoni, J. W. Krakauer, An implicit plan overrides an explicit strategy during visuomotor adaptation. *J. Neurosci.* **26**, 3642–3645 (2006).
13. J. A. Taylor, J. W. Krakauer, R. B. Ivry, Explicit and implicit contributions to learning in a sensorimotor adaptation task. *J. Neurosci.* **34**, 3023–3032 (2014).
14. T. Wang, J. A. Taylor, Implicit adaptation to mirror reversal is in the correct coordinate system but the wrong direction. *J. Neurophysiol.* **126**, 1478–1489 (2021).
15. S. A. Wilterson, J. A. Taylor, Implicit visuomotor adaptation remains limited after several days of training. *eNeuro* **8**, ENEURO.0312-20.2021 (2021).
16. G. Avraham, M. Keizman, L. Shmuelof, Environmental consistency modulation of error sensitivity during motor adaptation is explicitly controlled. *J. Neurophysiol.* **123**, 57–69 (2020).
17. T. Wang, G. Avraham, J. S. Tsay, S. J. Abram, R. B. Ivry, Perturbation variability does not influence implicit sensorimotor adaptation. *PLOS Comput. Biol.* **20**, e1011951 (2024).
18. G. Avraham, J. R. Morehead, H. E. Kim, R. B. Ivry, Reexposure to a sensorimotor perturbation produces opposite effects on explicit and implicit learning processes. *PLOS Biol.* **19**, e3001147 (2021).
19. D. Denny-Brown, Conditioned reflexes: An investigation of the physiological activity of the cerebral cortex. *Nature* **121**, 662–664 (1928).
20. H. Ebbinghaus, Memory: A contribution to experimental psychology. *Ann. Neurosci.* **20**, 155–156 (2013).
21. M. A. Smith, A. Ghazizadeh, R. Shadmehr, Interacting adaptive processes with different timescales underlie short-term motor learning. *PLOS Biol.* **4**, e179 (2006).
22. D. J. Herzfeld, Y. Kojima, R. Soetedjo, R. Shadmehr, Encoding of action by the Purkinje cells of the cerebellum. *Nature* **526**, 439–442 (2015).
23. L. S. Stone, S. G. Lisberger, Visual responses of Purkinje cells in the cerebellar flocculus during smooth-pursuit eye movements in monkeys. I. Simple spikes. *J. Neurophysiol.* **63**, 1241–1261 (1990).
24. J. F. Medina, S. G. Lisberger, Links from complex spikes to local plasticity and motor learning in the cerebellum of awake-behaving monkeys. *Nat. Neurosci.* **11**, 1185–1192 (2008).
25. D. Carulli, R. Broersen, F. de Winter, E. M. Muir, M. Mešković, M. de Waal, S. de Vries, H.-J. Boele, C. B. Canto, C. I. De Zeeuw, J. Verhaagen, Cerebellar plasticity and associative memories are controlled by perineuronal nets. *Proc. Natl. Acad. Sci. U.S.A.* **117**, 6855–6865 (2020).
26. J. L. Raymond, S. G. Lisberger, M. D. Mauk, The cerebellum: A neuronal learning machine? *Science* **272**, 1126–1131 (1996).
27. S. G. Lisberger, T. A. Pavelko, D. M. Broussard, Responses during eye movements of brain stem neurons that receive monosynaptic inhibition from the flocculus and ventral paraflocculus in monkeys. *J. Neurophysiol.* **72**, 909–927 (1994).
28. K. H. Lee, P. J. Mathews, A. M. B. Reeves, K. Y. Choe, S. A. Jami, R. E. Serrano, T. S. Otis, Circuit mechanisms underlying motor memory formation in the cerebellum. *Neuron* **86**, 529–540 (2015).
29. R. Apps, R. Hawkes, Cerebellar cortical organization: A one-map hypothesis. *Nat. Rev. Neurosci.* **10**, 670–681 (2009).
30. R. Apps, R. Hawkes, S. Aoki, F. Bengtsson, A. M. Brown, Cerebellar modules and their role as operational cerebellar processing units. *Cerebellum* **17**, 654–682 (2018).
31. J. B. Heald, M. Lengyel, D. M. Wolpert, Contextual inference underlies the learning of sensorimotor repertoires. *Nature* **600**, 489–493 (2021).
32. M. Haruno, D. M. Wolpert, M. Kawato, Hierarchical MOSAIC for movement generation. *Int. Congr. Ser.* **1250**, 575–590 (2003).
33. A. Collins, E. Koechlin, Reasoning, learning, and creativity: Frontal lobe function and human decision-making. *PLOS Biol.* **10**, e1001293 (2012).
34. M. Kawato, "Feedback-error-learning neural network for supervised motor learning," in *Advanced Neural Computers*, R. Eckmiller, Ed. (North-Holland, 1990), pp. 365–372.
35. D. Marr, A theory of cerebellar cortex. *J. Physiol.* **202**, 437–470 (1969).
36. D. M. Wolpert, R. C. Miall, M. Kawato, Internal models in the cerebellum. *Trends Cogn. Sci.* **2**, 338–347 (1998).
37. R. Apps, M. Garwicz, Anatomical and physiological foundations of cerebellar information processing. *Nat. Rev. Neurosci.* **6**, 297–311 (2005).
38. M. Junker, D. Endres, Z. P. Sun, P. W. Dicke, M. Giese, P. Thier, Learning from the past: A reverberation of past errors in the cerebellar climbing fiber signal. *PLOS Biol.* **16**, e2004344 (2018).
39. E. Sedaghat-Nejad, J. S. Pi, P. Hage, M. A. Fakharian, R. Shadmehr, Synchronous spiking of cerebellar Purkinje cells during control of movements. *Proc. Natl. Acad. Sci. U.S.A.* **119**, e2118954119 (2022).
40. F. A. Miles, S. G. Lisberger, Plasticity in the vestibulo-ocular reflex: A new hypothesis. *Annu. Rev. Neurosci.* **4**, 273–299 (1981).
41. T. Ohyama, W. L. Nores, J. Medina, F. Riusech, M. Mauk, Learning-induced plasticity in deep cerebellar nucleus. *J. Neurosci.* **26**, 12656–12663 (2006).
42. M. D. Mauk, Roles of cerebellar cortex and nuclei in motor learning: Contradictions or clues? *Neuron* **18**, 343–346 (1997).
43. T. Ohyama, W. L. Nores, M. Murphy, M. D. Mauk, What the cerebellum computes. *Trends Neurosci.* **26**, 222–227 (2003).
44. S. Ono, V. E. Das, M. J. Mustari, Role of the dorsolateral pontine nucleus in short-term adaptation of the horizontal vestibuloocular reflex. *J. Neurophysiol.* **89**, 2879–2885 (2003).
45. J. F. Medina, K. S. Garcia, W. L. Nores, N. M. Taylor, M. D. Mauk, Timing mechanisms in the cerebellum: Testing predictions of a large-scale computer simulation. *J. Neurosci.* **20**, 5516–5525 (2000).
46. K. S. Garcia, M. D. Mauk, Pharmacological analysis of cerebellar contributions to the timing and expression of conditioned eyelid responses. *Neuropharmacology* **37**, 471–480 (1998).
47. D. J. Herzfeld, N. J. Hall, M. Tringides, S. G. Lisberger, Principles of operation of a cerebellar learning circuit. *eLife* **9**, e55217 (2020).
48. R. Shadmehr, Population coding in the cerebellum: A machine learning perspective. *J. Neurophysiol.* **124**, 2022–2051 (2020).
49. J. F. Medina, M. D. Mauk, Simulations of cerebellar motor learning: Computational analysis of plasticity at the mossy fiber to deep nucleus synapse. *J. Neurosci.* **19**, 7140–7151 (1999).
50. J. F. Medina, M. D. Mauk, Computer simulation of cerebellar information processing. *Nat. Neurosci.* **3**, 1205–1211 (2000).
51. H. E. Kim, G. Avraham, R. B. Ivry, The psychology of reaching: Action selection, movement implementation, and sensorimotor learning. *Annu. Rev. Psychol.* **72**, 61–95 (2021).
52. G. Avraham, J. A. Taylor, A. Breska, R. B. Ivry, S. D. McDougle, Contextual effects in sensorimotor adaptation adhere to associative learning rules. *eLife* **11**, e75801 (2022).
53. J. S. Tsay, D. E. Parvin, R. B. Ivry, Continuous reports of sensed hand position during sensorimotor adaptation. *J. Neurophysiol.* **124**, 1122–1130 (2020).
54. P. M. Bays, J. R. Flanagan, D. M. Wolpert, Interference between velocity-dependent and position-dependent force-fields indicates that tasks depending on different kinematic parameters compete for motor working memory. *Exp. Brain Res.* **163**, 400–405 (2005).
55. G. Lerner, S. Albert, P. A. Caffaro, J. I. Villalta, F. Jacobacci, R. Shadmehr, V. Della-Maggiore, The origins of anterograde interference in visuomotor adaptation. *Cereb. Cortex* **30**, 4000–4010 (2020).

56. T. Brashers-Krug, R. Shadmehr, E. Bizzi, Consolidation in human motor memory. *Nature* **382**, 252–255 (1996).
57. L.-A. Leow, G. Hammond, A. de Rugy, Anodal motor cortex stimulation paired with movement repetition increases anterograde interference but not savings. *Eur. J. Neurosci.* **40**, 3243–3252 (2014).
58. G. C. Sing, M. A. Smith, Reduction in learning rates associated with anterograde interference results from interactions between different timescales in motor adaptation. *PLOS Comput. Biol.* **6**, e1000893 (2010).
59. J. B. Heald, M. Lengyel, D. M. Wolpert, Contextual inference in learning and memory. *Trends Cogn. Sci.* **27**, 43–64 (2023).
60. J. N. Ingram, J. R. Flanagan, D. M. Wolpert, Context-dependent decay of motor memories during skill acquisition. *Curr. Biol.* **23**, 1107–1112 (2013).
61. I. S. Howard, D. M. Wolpert, D. W. Franklin, The value of the follow-through derives from motor learning depending on future actions. *Curr. Biol.* **25**, 397–401 (2015).
62. I. S. Howard, D. M. Wolpert, D. W. Franklin, The effect of contextual cues on the encoding of motor memories. *J. Neurophysiol.* **109**, 2632–2644 (2013).
63. S. D. McDougle, K. M. Bond, J. A. Taylor, Explicit and implicit processes constitute the fast and slow processes of sensorimotor learning. *J. Neurosci.* **35**, 9568–9579 (2015).
64. K. A. Day, R. T. Roemmich, J. A. Taylor, A. J. Bastian, Visuomotor learning generalizes around the intended movement. *eNeuro* **3**, ENEURO.0005-16.2016 (2016).
65. J. R. Morehead, S. E. Qasim, M. J. Crossley, R. Ivry, Savings upon re-aiming in visuomotor adaptation. *J. Neurosci.* **35**, 14386–14396 (2015).
66. E. Zarahn, G. D. Weston, J. Liang, P. Mazzoni, J. W. Krakauer, Explaining savings for visuomotor adaptation: Linear time-invariant state-space models are not sufficient. *J. Neurophysiol.* **100**, 2537–2548 (2008).
67. D. J. Herzfeld, P. A. Vaswani, M. K. Marko, R. Shadmehr, A memory of errors in sensorimotor learning. *Science* **345**, 1349–1353 (2014).
68. P. W. Frey, L. E. Ross, Classical conditioning of the rabbit eyelid response as a function of interstimulus interval. *J. Comp. Physiol. Psychol.* **65**, 246–250 (1968).
69. J. W. Krakauer, C. Ghez, M. F. Ghilardi, Adaptation to visuomotor transformations: Consolidation, interference, and forgetting. *J. Neurosci.* **25**, 473–478 (2005).
70. K. P. Kording, J. B. Tenenbaum, R. Shadmehr, The dynamics of memory as a consequence of optimal adaptation to a changing body. *Nat. Neurosci.* **10**, 779–786 (2007).
71. J. F. Medina, W. L. Nores, T. Ohyama, M. D. Mauk, Mechanisms of cerebellar learning suggested by eyelid conditioning. *Curr. Opin. Neurobiol.* **10**, 717–724 (2000).
72. J. L. Raymond, J. F. Medina, Computational principles of supervised learning in the cerebellum. *Annu. Rev. Neurosci.* **41**, 233–253 (2018).
73. H. E. Kim, J. R. Morehead, D. E. Parvin, R. Moazzezi, R. B. Ivry, Invariant errors reveal limitations in motor correction rather than constraints on error sensitivity. *Commun. Biol.* **1**, 19 (2018).
74. K. Wei, K. Körding, Relevance of error: What drives motor adaptation? *J. Neurophysiol.* **101**, 655–664 (02/2009).
75. J. S. Tsay, G. Avraham, H. E. Kim, D. E. Parvin, Z. Wang, R. B. Ivry, The effect of visual uncertainty on implicit motor adaptation. *J. Neurophysiol.* **125**, 12–22 (2021).
76. S. A. Hutter, J. A. Taylor, Relative sensitivity of explicit reaiming and implicit motor adaptation. *J. Neurophysiol.* **120**, 2640–2648 (2018).
77. J. S. Tsay, R. B. Ivry, A. Lee, G. Avraham, Moving outside the lab: The viability of conducting sensorimotor learning studies online. *Neurons Behav. Data Anal. Theory* **5**, 10.51628/001c.26985 (2021).
78. D. J. Herzfeld, Y. Kojima, R. Soetedjo, R. Shadmehr, Encoding of error and learning to correct that error by the Purkinje cells of the cerebellum. *Nat. Neurosci.* **21**, 736–743 (2018).
79. L. Moscato, I. Montagna, L. De Propris, S. Tritto, L. Mapelli, E. D'Angelo, Long-lasting response changes in deep cerebellar nuclei in vivo correlate with low-frequency oscillations. *Front. Cell. Neurosci.* **13**, 84 (2019).
80. J. F. Medina, K. S. Garcia, M. D. Mauk, A mechanism for savings in the cerebellum. *J. Neurosci.* **21**, 4081–4089 (2001).
81. J. F. Medina, J. C. Repa, M. D. Mauk, J. E. LeDoux, Parallels between cerebellum- and amygdala-dependent conditioning. *Nat. Rev. Neurosci.* **3**, 122–131 (2002).
82. A. M. Hadjiosif, J. R. Morehead, M. A. Smith, A double dissociation between savings and long-term memory in motor learning. *PLOS Biol.* **21**, e3001799 (2023).
83. C. I. De Zeeuw, T. J. Ruigrok, Olivary projecting neurons in the nucleus of Darkschewitsch in the cat receive excitatory monosynaptic input from the cerebellar nuclei. *Brain Res.* **653**, 345–350 (1994).
84. J. Turecek, W. G. Regehr, Cerebellar and vestibular nuclear synapses in the inferior olive have distinct release kinetics and neurotransmitters. *eLife* **9**, e61672 (2020).
85. J. F. Medina, W. L. Nores, M. D. Mauk, Inhibition of climbing fibres is a signal for the extinction of conditioned eyelid responses. *Nature* **416**, 330–333 (2002).
86. F. Bengtsson, G. Hesslow, Cerebellar control of the inferior olive. *Cerebellum* **5**, 7–14 (2006).
87. J. S. Tsay, C. Irving, R. B. Ivry, Signatures of contextual interference in implicit sensorimotor adaptation. *Proc. Biol. Sci.* **290**, 20222491 (2023).
88. A. G. E. Collins, The tortoise and the hare: Interactions between reinforcement learning and working memory. *J. Cogn. Neurosci.* **30**, 1422–1432 (2017).
89. A. G. E. Collins, S. D. McDougle, Context is key for learning motor skills. *Nature* **600**, 387–388 (2021).
90. D. J. Herzfeld, R. Shadmehr, Cerebellum estimates the sensory state of the body. *Trends Cogn. Sci.* **18**, 66–67 (2014).
91. L. N. Gonzalez Castro, A. M. Hadjiosif, M. A. Hemphill, M. A. Smith, Environmental consistency determines the rate of motor adaptation. *Curr. Biol.* **24**, 1050–1061 (2014).
92. W. Zhou, J. Fitzgerald, K. Colucci-Chang, K. G. Murthy, W. M. Joiner, The temporal stability of visuomotor adaptation generalization. *J. Neurophysiol.* **118**, 2435–2447 (2017).
93. J. W. Krakauer, P. Mazzoni, A. Ghazizadeh, R. Ravindran, R. Shadmehr, Generalization of motor learning depends on the history of prior action. *PLOS Biol.* **4**, e316 (2006).
94. T. Wang, J. Li, R. B. Ivry, Attention defines the context for implicit sensorimotor adaptation. *J. Neurosci.* **45**, e0117252025 (2025). https://doi.org/10.1523/JNEUROSCI.0117-25.2025.
95. M. Negrello, P. Warnaar, V. Romano, C. B. Owens, S. Lindeman, E. Iavarone, J. K. Spanke, L. W. J. Bosman, C. I. De Zeeuw, Quasiperiodic rhythms of the inferior olive. *PLOS Comput. Biol.* **15**, e1006475 (2019).
96. S. Loyola, T. M. Hoogland, H. Hoedemaker, V. Romano, M. Negrello, C. I. De Zeeuw, How inhibitory and excitatory inputs gate output of the inferior olive. *eLife* **12**, e83239 (2023).
97. Y. Baumel, G. A. Jacobson, D. Cohen, Implications of functional anatomy on information processing in the deep cerebellar nuclei. *Front. Cell. Neurosci.* **3**, 14 (2009).
98. O. A. Kim, S. Ohmae, J. F. Medina, A cerebello-olivary signal for negative prediction error is sufficient to cause extinction of associative motor learning. *Nat. Neurosci.* **23**, 1550–1554 (2020).
99. H. P. Op de Beeck, C. I. Baker, The neural basis of visual object learning. *Trends Cogn. Sci.* **14**, 22–30 (2010).
100. D. Narain, E. D. Remington, C. I. D. Zeeuw, M. Jazayeri, A cerebellar mechanism for learning prior distributions of time intervals. *Nat. Commun.* **9**, 469 (2018).
101. T. Wang, Y. Luo, R. B. Ivry, J. S. Tsay, E. Pöppel, Y. Bao, A unitary mechanism underlies adaptation to both local and global environmental statistics in time perception. *PLOS Comput. Biol.* **19**, e1011116 (2023).
102. J. R. Pugh, I. M. Raman, Mechanisms of potentiation of mossy fiber EPSCs in the cerebellar nuclei by coincident synaptic excitation and inhibition. *J. Neurosci.* **28**, 10549–10560 (2008).
103. W. Zhang, D. J. Linden, Long-term depression at the mossy fiber-deep cerebellar nucleus synapse. *J. Neurosci.* **26**, 6935–6944 (2006).
104. J. R. Pugh, I. M. Raman, Potentiation of mossy fiber EPSCs in the cerebellar nuclei by NMDA receptor activation followed by postinhibitory rebound current. *Neuron* **51**, 113–123 (2006).
105. M. Ito, M. Kano, Long-lasting depression of parallel fiber-Purkinje cell transmission induced by conjunctive stimulation of parallel fibers and climbing fibers in the cerebellar cortex. *Neurosci. Lett.* **33**, 253–258 (1982).
106. D. Marr, W. T. Thach, "A theory of cerebellar cortex," in *From the Retina to the Neocortex* (Birkhäuser Boston, 1991), pp. 11–50.
107. A. R. Best, W. G. Regehr, Inhibitory regulation of electrically coupled neurons in the inferior olive is mediated by asynchronous release of GABA. *Neuron* **62**, 555–565 (2009).
108. R. Shadmehr, F. A. Mussa-Ivaldi, Adaptive representation of dynamics during learning of a motor task. *J. Neurosci.* **14**, 3208–3224 (1994).
109. T. Wang, G. Avraham, J. S. Tsay, T. Thummala, R. B. Ivry, Advanced feedback enhances sensorimotor adaptation. *Curr. Biol.* **34**, 1076–1085.e5 (2024).
110. T. Wang, R. J. Morehead, J. S. Tsay, R. B. Ivry, The origin of movement biases during reaching. *eLife* **14**, e100715 (2025). https://doi.org/10.7554/eLife.100715.1.

Acknowledgments: We thank J. Medina, C. Miall, D. Wolpert, M. Lengyel, and E. Guigon for discussions. **Funding:** This work was funded by the National Institutes of Health grant nos. NS116883 and NS105839 (R.B.I.). **Author contributions:** Conceptualization: T.W. and R.B.I. Methodology: T.W. and R.B.I. Software: T.W. Validation: T.W. Formal analysis: T.W. Investigation: T.W. Resources: R.B.I. Data curation: T.W. Writing—original draft: T.W. Writing—review and editing: T.W. and R.B.I. Visualization: T.W. Supervision: R.B.I. Project administration: T.W. and R.B.I. Funding acquisition: R.B.I. **Competing interests:** R.B.I. is a cofounder with equity in Magnetic Tides Inc. All other authors declare that they have no competing interests. **Data and materials availability:** All data needed to evaluate the conclusions in the paper are present in the paper and/or the Supplementary Materials. The data and code supporting this work are available at https://zenodo.org/records/14241549.

Submitted 3 July 2024
Accepted 26 September 2025
Published 29 October 2025
10.1126/sciadv.adr4540